Chapter 4

Coordination driven self-assembly of 1,3-bis(2-(alkylamino)acetamido)phenylene, CS_2 and Ni^{II}, Cu^{II} or Zn^{II}:Synthesis, spectroscopic, DFT, crystallographic and cytotoxic study

Abstract

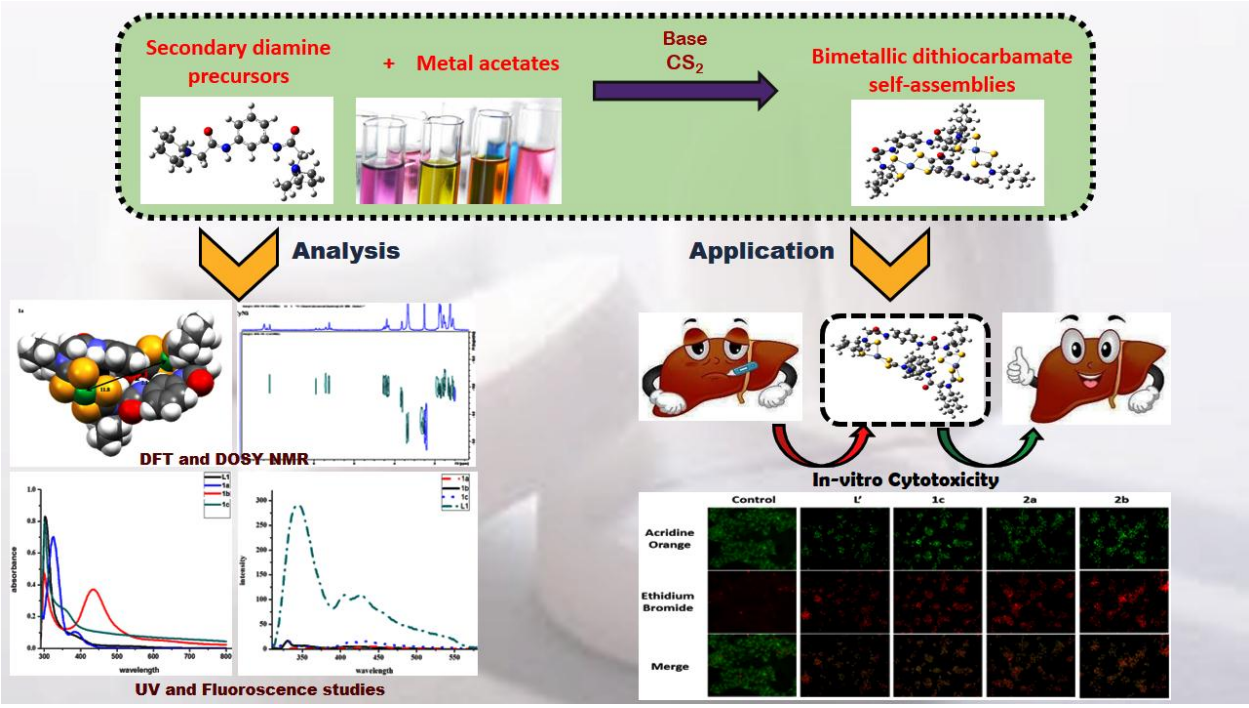

α-chloroamide 1,3-bis(2-chloroacetamido)phenylene (**L'**) is selected as a lead compound to derive three organic diamine derivatives *ca* 1,3-bis(2-(cyclohexylamino)acetamido)phenylene (**L^1**), 1,3-bis(2-(isopropylamino)acetamido)phenylene (**L^2**) and 1,3-bis(2-(n-butylamino)acetamido) phenylene (**L^3**). A programmed self-assembly involving L^1-L^3, CS_2 and Ni^{II}, Cu^{II} or Zn^{II} ions affords a novel series of 32-membered neutral binuclear metallomacrocyclic

dithiocarbamate complexes of the type $[M^{II}_2$-μ^2-bis-{(κ^2*S*,*S*-$S_2CN(R)CH_2CONH)_2C_6H_4$}] {R = *Cy*, M = Ni^{II} **1a**, Cu^{II} **1b**, Zn^{II} **1c**; R = ^{i}*Pr*, M = Ni^{II} **2a**, Cu^{II} **2b**, Zn^{II} **2c**; R = ^{n}*Bu*, M = Ni^{II} **3a**, Cu^{II} **3b**, Zn^{II} **3c**}. All the compounds were characterized by spectroscopic (^{1}H, ^{13}C, DEPT 135, ^{1}H DOSY NMR, ESI MS, UV-visible absorption, emission, IR) and by thermogravimetric methods. Interestingly, X-ray structure of L' demonstrates propensity of formation of an unusual C-Cl…π intermolecular contacts along with C-H…Cl, CH...O and N-H...O that lead to a fascinating 2D infinite supramolecular molecular sheet. All the compounds were screened for their *in vitro* cytotoxic activity against malignant tumor Hep G2 (hepatoma) cell line by the MTT assay. A majority of compounds *ca* **L', L^1, 1a, 1b, 1c, 2a, 2b, 2c, L^3,3a, 3b, 3c** display IC_{50} values lower than Cisplatin and specificity for carcinoma Hep G2 over normal liver cell line (WRL-68). Evidently cytotoxic potentials of L^1-L^3 improved tremendously upon formation of their corresponding bimetallic dithiocarbamate complexes **1a-1c, 2a-2c, 3a-3c**, apparently due to presence of several biologically relevant groups such as amide, sulfur and transition metal ions onto a single molecular platform which jointly accelerate their cytotoxic activity. The shrinking of cells can be clearly visualized by acridine orange/ethidium bromide (AO/EB) staining indicating the induction of apoptosis as part of the mechanism of action of these compounds. Further, DFT level calculations have been performed on representative compounds to reinforce the experimental results.

4.1 Introduction

Over the period of time considerable amount of work has been diverted towards the building of effectual macrocyclic chemo-therapeutic motif bearing the properties of drugs or as potent drug-delivery agents.[1,2] However, the success of these compounds as effective chemotherapeutic agents is majorly constrained by the lack of apt structural alteration, difficulties in transportation, exclusive selectivity for the target site and retention of the required chemical structure of the pharmacophore within the biological environment. Transition metals exhibiting variable coordination numbers, redox states, thermodynamic-kinetic characteristics and geometries contribute greatly towards the

development of a single molecular platform bearing biologically active groups through coordination driven self-assembly that offers additional opportunities for development of new therapeutic agents not accessible to organic compounds.[3] Literature reveals sulfurs are an important constituent of biomolecules, plays a crucial role in transporting and addressing the molecule to the targets as well as in the protection of the pharmacophore against untimely exchanges with biomolecules.[4,5] Compounds with sulfur-rich ligands exhibit good DNA/protein binding/cleaving and catalytic activity toward glutathione [6] besides their wide range of applications in the area of electrical conductivity, molecular magnetism, electrochemical, biological processes, optoelectronic properties and biological processes.[7,8] A class of sulfur rich ligands viz. dithiocarbamates have been effectively used in assembling diverse transition metal and main-group ions into a wide variety of discrete supramolecular species including macrocycles, cavitands, cryptands, catenanes and container molecules.[9] Such supramolecular structures have been well studied to encapsulate and stabilize a number of guest substrates, however their explorations from medicinal perspectives are scarcely been investigated.[10, 25]

Nature and synthetic chemists have demonstrated the significance of amides as an important building blocks.[11] In particular α-chloroamides have been used as valuable synthons for the development of stable lanthanide-based macrocycles for biological applications.[12] Professor T. Gunnlaugsson and his research group [13] have used a varieties of α-chloroamidesto derives macrocyclic lanthanide cyclen complexes which have largely been used as potential MRI contrast agents and as ribonuclease mimics.[12–14] Pharmacological and biochemical studies further reveal that fatty acid amides act as biological lipids, found in ceramides, sphingo lipids and some compounds of brain and other tissues.[15] Very recently, an anchording effect of amide bonds induced fast electron transfer and strong chemical bonding that result in enhanced amount of immobilized glucose oxidase (GOx) and performance of enzymatic biofuel cell (EBC) have been reported by Kwon and his co-workers.[16] The relevance of amide group in glycine amide derivatives as novel Vascular Adhesion Protein-1 inhibitors have also been reported by Yamaki el al.[17] Moreover, reports on phenylene derivatives showing therapeutic effects include chalcogen functionalized phenylene derivative 1,4-phenylene bis(methylene)

selenocyanate (p-XSC)[18] and poly(p-phenylene) that are indeed widely used for various biological applications through enhanced interaction with the target sites.[19-21]

In the light of these observations and towards our ongoing interest in exploring binuclear metallomacrocyclic ditiocarbamate complexes with better hepatocytotoxic potentials,[10,25] we have selected a known α-chloroamides ca 1,3-bis(2-chloroacetamido)phenylene (**L'**) to derive a new series of organic diamine derivatives ca 1,3-bis(2-(cyclohexylamino)acetamido)phenylene (**L^1**), 1,3-bis(2-(isopropylamino)acetamido)phenylene (**L^2**) and 1,3-bis(2-(n-butylamino)acetamido) phenylene (**L^3**). These diamines have been subsequently used in a programmed self-assembly with CS_2 and transition metal ions affords the novel series of 32-membered neutral binuclear metallomacrocyclic dithiocarbamate complexes of the type [M^{II}_2-μ^2-bis-{(κ^2*S,S*-$S_2CN(R)CH_2CONH)_2C_6H_4$}] which holds several pendant amide groups into the macrocyclic framework. It is anticipated that the presence of several biological relevant groups such as amide, dithioand transition metal ions onto a single molecular platform would jointly accelerate the biological relevance of these complexes.

4.2 Experimental Section

4.2.1 Instrumentation

All the A. R. grade chemicals such as metal acetates, reagents and solvents were obtained from different sources and have been used without further purification.Reactions and manipulations were performed under an inert atmosphere. Melting points were recorded in open capillaries and uncorrected. Thin Layer Chromatography was performed on Merck 60 F254 aluminum coated plates. Mass spectra were obtained on AB SCIEX 3200 Q TRAP LCMS instrument. FT-IR (KBr pellets) spectra were recorded in the 4000-400 cm^{-1} range using a Perkin-Elmer FT-IR spectrometer. The NMR spectra were obtained on a Bruker AV-III 400 MHz spectrometer in $CDCl_3$/d^6-DMSO solvents as per the solubility and values are reported in parts per million (ppm). UV-visible absorption spectra were recorded on a Perkin Elmer Lambda 35 UV-visible spectrophotometer. Fluorescence was recorded on JASCO make

spectrofluorometer model FP-6300 and thermal study was performed by using SII TG/DTA 6300 in flowing N_2 with a heating rate of 10 °C min^{-1}.

4.2.2 Preparation of 1, 3-bis(2-chloroacetamido)phenylene (L')

To a dichloromethane solution of 1 equivalent m-phenylenediamine (0.5 g; 2.05 mmol), 3 equivalents of solid $NaHCO_3$ (0.517 g; 6.15 mmol) was added and the reaction mixture was stirred for 30 minutes. To this solution, 2.5 equivalents of 2-chloroacetyl chloride (0.578 g; 5.12 mmol) was added carefully drop wise by using dropping funnel at 0-5 ˚C over a period of 40 minutes and then allowed to stir at room temperature for 2-3 hours. The progress of reaction was monitored by TLCs. The solid residue was filtered off over glass sintered crucible, washed with 5 × 8 mL of 5% $NaHCO_3$ solution followed by 3 × 10 mL of distilled water and then by hexane to yield 1,3-bis(2-chloroacetamido)phenylene **(L')**which was thoroughlydried under high vacuum and the product was taken for analysed.

L': MW: 260.01,Yield: 485.2 g, 91 %.M.p. 220°C dec.^{1}H NMR (400 MHz, DMSO-d_6): δ (ppm) 10.75 (s, 2H, -CON*H*); 7.95 (m, 1H), 7.37-7.39 (m, 2H), 7.24 (t, 1H); 4.31 (s, 4H, NCH_2CO).

4.2.3 General method of preparation of secondary diamine precursors 1,3-bis(alkylamino)acetamido)phenylene L^1-L^3

An excess amount of cyclohexyl amine (892.2 mg, 9 mmol), isopropylamine (531.9 mg, 9 mmol) or n-butylamine (658.2 mg, 9 mmol), was added to a ethanolic solution of 1,3-bis(2-chloroacetamido)phenylene (0.522 g, 2 mmol). The reaction mixture was refluxed in the presence of catalytic amount of Et_3N for 8 hours and the progress of reaction was examined by thin layer chromatography. The reaction mixture was cooled at room temperature and further chilled by adding ice to get precipitate which was filtered, washed with cold water, followed by n-hexane and diethyl ether to produce diamines**L^1-L^3** in good yields. The samples were stored under a atmosphere of $N_2$and taken for analysis.

1,3-bis(2-(cyclohexylamino)acetamido)phenylene (L^1): MW: 386.53, Yield: 0.664 g, 86%, m.p. 70 °C dec. (close to DTA peak).ES-MS: 386.1(M^+). Infrared spectrum (KBr disc, cm^{-1}): 3432.00w, 3330.97m, 3285.92w, 3087.54w, 3030.29w, 2926.94vs, 2851.59s, 2796.87w, 2660.21w, 2592.69w, 2360.02m, 2337.13w, 1939.71w, 1854.91w, 1766.24w, 1727.30w, 1692.48s, 1652.02vs, 1611.18s, 1546.27s, 1533.50vs, 1447.93vs, 1412.13m, 1371.49m, 1348.04w, 1285.95w, 1230.64w, 1186.51w, 1136.47m, 1031.32w, 953.68w, 927.41w, 891.70m, 827.41w, 788.58m, 690.18w, 657.04w, 608.81w, 576.57w, 539.18w, 496.83w, 453.76w. ^{1}HNMR (400 MHz, DMSO-d_6): δ (ppm) 9.90 (s, 4H, -CON*H*); 7.92-7.21 (m, 4*H*, Ph); 3.34 (s, 4H, NCH_2CO); 2.32 (m, 2H, NC*H* of Cy); 1.85 (s, br, 2H, N*H*); 1.81-1.03 (m, 20H, *Cy*). ^{13}C NMR (400 MHz, DMSO-d_6): δ (ppm) δ 172.2(*C*=O), 139.38 (*C*-N), 129.52, 114.49, 110.12(*Ph*), 56.6(*C*HofCy), 50.6 (N*C*H_2CO), 36.25, 33.8, 31.22, 26.1, 25.0(*C*H_2 of Cy).DEPT 135(400 MHz, DMSO-d6):δ (ppm) δ 129.65, 114.48, 110.12 (*Ph*), 56.66 (*C*H of Cy), 50.65 (N*C*H_2CO), 35.76, 33.37, 26.19, 25.78, 24.99 (*C*H_2 of Cy).

1, 3-bis(2-(isopropylamino)acetamido)phenylene (L^2): MW: 306.40, Yield: 0.502g, 82%. m.p. 82 °C dec.ES-MS: 307.2 (M+H). Infrared spectrum (KBr disc, cm^{-1}): 3520.02w, 3288.37s, 3010.76w, 2965.87vs, 2929.28sh, 2615.80w, 1690.95vs, 1665.93vs, 1607.17vs, 1529.98vs, 1492.33s, 1448.31s, 1419.31s, 1383.62w, 1368.49w, 1309.32m, 1261.52w, 1217.38m, 1173.46m, 1133.42m,1088.85w, 1002.17w, 925.59w, 875.03w, 783.98m, 757.11vs, 690.42w, 665.69w, 484.01m, 469.19m, 453.71m, 444.04m. ^{1}H NMR (400 MHz, DMSO-d_6): δ (ppm) 9.85(s, 4H, CON*H*); 7.62-6.92(m,4H,*Ph*); 3.40(s,4H, NCH_2CO); 2.74(m, 2H, C*H* of ^{i}*Pr*); 2.49 (s, br, 2H, N*H*, merged with DMSO) 1.00(d,12H,-CH_3).^{13}C NMR:(400 MHz, DMSO-d6) δ ppm: 170.90,152.98(*C*=O); 134.61 (*C*-N), 121.23, 119.16 (*Ph*) ; 50.91 (N*C*H_2CO); 48.69 (*C*H of ^{i}Pr); 23.11 (CH_3). DEPT 135(400 MHz, DMSO-d6):129.50, 114.54, 110.21 (*Ph*) ; 51.01 (N*C*H_2CO); 48.68 (*C*H of ^{i}Pr); 23.19 (CH_3).

1, 3-bis(2-(n-butylamino)acetamido)phenylene (L^3): MW: 334.46, Yield: 0.581 g, 87%.m.p. 48°C dec.ES-MS: 335.2 (M+H). Infrared spectrum (KBr disc, cm^{-1}): 3519.97w, 3285.14vs, 3083.06sh, 2956.30vs, 2927.47vs, 2871.40vs, 2443.56w, 1856.85m, 1690.82vs, 1669.52vs, 1608.87vs, 1565.38m, 1547.63vs, 1532.05vs, 1487.96

m, 1416.88vs, 1378.03m, 1303.10s, 1229.43s, 1163.82m, 1129.24s, 1044.64w, 997.43w, 960.17w, 875.74m, 782.98s, 735.68w, 689.29m, 556.85w, 492.79m, 454.53m. ^{1}H NMR (400 MHz, DMSO-d_6): δ (ppm) 9.81(s, 4H, CON*H*); 7.94(s, 1H,*Ph*); 7.31 (d, 2H, *Ph*), 7.2 (t, 1H,*Ph*); 3.36 (s,4H,NCH_2CO);2.2 (broad s, 2H, N*H*); 1.980 (s, 4H, NCH_2 of ^{n}*Bu*); 1.44 (m, 8H, CH_2 of ^{n}*Bu*); 1.44-1.34(m, 6H, CH_3 of ^{n}*Bu*).^{13}C NMR (400 MHz, DMSO-d_6): δ (ppm) 170.7(*C*=O), 139.4 (*C*-N); 129.4, 114.6, 110.3(*Ph*), 53.1 (N*CH*$_2$CO), 49.1(NCH$_2$ of ^{n}*Bu*), 32.0, 20.3(*C*H$_2$ of ^{n}*Bu*); 14.3 (*C*H$_3$ of ^{n}*Bu*). DEPT-135 (400 MHz, DMSO-d6): δ ppm 129.47, 114.55, 110.25 (*Ph*), 53.26 (N*CH*$_2$CO), 49.25 (NCH$_2$ of ^{n}*Bu*), 32.03, 20.34 (*C*H$_2$ of ^{n}*Bu*); 14.37 (*C*H$_3$ of ^{n}*Bu*).

4.2.4 General Synthetic procedure for metallomacrocyclic dithiocarbamate complexes 1a-1c, 2a-2c, 3a-3c

A surplus amount of NaOH (~3 equivalent; ~ 0.060 g) and carbon disulfide (~10 equivalent; ~ 0.5 ml) were added to a acetonitrile solution of 1 equivalent of respective diamine precursor **L^{1}** (0.193 g, 0.5mmol), **L^{2}** (0.153g, 0.5mmol) or **L^{3}** (0.167g, 0.5mmol), with fast stirring. The stirring was continued for 12 h at room temperature. In this course of time, a change in color wasobserved from colorless to pale yellow. To this reaction mixture,Ni^{II}($C_2H_3O_2$)$_2$.4H_2O (136 mg, 0.55mmol), Cu($C_2H_3O_2$)$_2$.H_2O (0.111 g, 0.55 mmol)or Zn^{II}($C_2H_3O_2$)$_2$.2H_2O (121 mg, 0.55mmol), dissolved in minimum quantity of distilled water, was added with rigorous stirring and the reaction was allowed to continue for 8 h at room temperature. The reaction mixture was vacuum dried. The residue was given repeated washings of distilled water, followed by n-hexane and diethyl ether. Corresponding products **1a-1c, 2a-2c, 3a-3c** obtained was dried under vacuum.

[Ni$_2$-*μ*^{2}-bis-{(*κ*^{2}*S*,*S*-S_2CN(Cy)CH_2CONH)$_2$$C_6H_4$}] (1a). Green; MW: 1190.98, Yield: *ca* 0.232 g, 78%.m.p. >230 °C dec.ES-MS: 1191.4 (M+H). Infrared spectrum(KBr disc, cm^{-1}): 3284.88m, 2933.83s, 2854.74m, 1681.98s, 1606.76m, 1541.18m, 1477.52s, 1458.23s, 1417.73m, 1323.21w, 1303.92w, 1280.78w, 1267.27w, 1242.20w , 1224.84w, 1193.98w, 1166.97w, 1139.97w, 1010.73w, 972.16w, 895.00w, 785.05w, 688.61w, 623.03w, 518.87w, 451.36w. ^{1}H NMR (400 MHz, DMSO-d_6): δ (ppm)10.484. 10.21 (s, 4H,

CON*H*), 7.526-7.125 (m, 8H, *Ph*), 4.477 (m, 8H, NCH_2CO), 3.612 (s, 4H, C*H* of *Cy*), 1.744 -1.074 (m, 20H,*Cy*). ^{13}C NMR (400 MHz, DMSO-d6): δ (ppm): 204.1 **(-N^{13}*C*S$_2$)**, 164.7 (C=O), 139.4 (C-N), 129.6, 114.5, 110.01 (*Ph*), 59.28(*C*H of *Cy*), 53.2, 48.2 (N*C*H$_2$CO),31.6, 29.3, 25.4, 25.1, 24.8,24.6 (*C*H$_2$ of Cy).

[Cu$_2$-*μ*^{2}-bis-{(*κ*^{2}*S,S*-S$_2$CN(Cy)CH$_2$CONH)$_2$C$_6$H$_4$}] (1b). Brown; MW: 1200.68, Yield: ca 0.177 g, 59 %; m.p. 258 °C dec. ES-MS: 1200.3 (M^+). Infrared spectrum (KBrdisc, cm^{-1}): 3300 broad w, 2933.83s, 2856.67m, 2112.12w, 1737.92w, 1681.98m, 1606.76m, 1546.96m, 1471.74s, 1454.38s, 1240.27m, 1211.34m, 1168.90s, 1138.04m, 1114.89m, 1051.24m, 893.07w, 788.91w, 888.61w, 819.17w, 518.87w, 451.36w.

[Zn$_2$-*μ*^{2}-bis-{(*κ*^{2}*S,S*-S$_2$CN(Cy)CH$_2$CONH)$_2$C$_6$H$_4$}] (1c). Pale Yellow; MW: 1204.35,Yield: ca 0.196 g, 65%; m.p. 241 °C dec.ES-MS: 1205.0 (M+H). Infrared spectrum(KBr disc, cm^{-1}):3292.60m, 2931.90s, 2854.74m, 1683.91s, 1606.76m, 1543.10m, 1535.39m, 1489.10m, 1452.45s, 1410.01m, 1323.21w, 1307.78w, 1240.27w, 1166.97w, 1008.80w, 972.16w, 887.28w, 783.13w, 688.61w, 518.87w, 474.50w.^{1}H NMR (400 MHz, DMSO-d$_6$) : δ (ppm) 10.226, 10.054 (s, 4H, -CON*H*); 7.940-6.888(m, 8H, *Ph*); 4.795(s, 8H, NCH_2CO); 4.542 (broad s, 4H, C*H* of Cy); 1.817-1.095 (m, 20H, *Cy*).^{13}C NMR(400 MHz, DMSO-d$_6$) : δ (ppm) 206.2, 203.55 **(-N^{13}CS$_2$)**, 166.2, 165.93, 164.53 (C=O), 140.9, 139.9, 139.8 (*C*-N); 129.6, 129.3 114.2, 110.5(*Ph*), 64.08(N*C*H$_2$CO); 53.35, 51.9(*C*H of *Cy*); 31.6, 30.0, 25.7, 25.1(*C*H$_2$ of Cy).

[Ni$_2$-*μ*^{2}-bis-{(*κ*^{2}*S,S*-S$_2$CN(*^{i}Pr*)CH$_2$CONH)$_2$C$_6$H$_4$}] (2a). Green; MW: 1030.72, Yield: *ca*0.118 g, 46%; m.p. 262 °C dec. ES-MS: 1030.4 (M^+). ^{1}H NMR (400 MHz, DMSO-d6): δ (ppm) 10.145 (s,4H,N*H*), 7.895-7.119 (m,8H,*Ph*), 4.543, 4.225 (NCH_2CO), 3.244 (s, 4H, C*H* of ^{i}Pr), 1.047 (s, 24H, CH_3). ^{13}C NMR (400 MHz, DMSO-d6) δ (ppm): 206.7 **(-N^{13}*C*S$_2$)**, 164.7 (*C*=O); 139.4 (*C*-N), 129.6, 114.6, 113.8, 110.2, (*Ph*), 51.3 (N*C*H$_2$CO), 47.6 (CH of *^{i}Pr*), 19.3, (CH$_3$ of *^{i}Pr*).

[Cu$_2$-*μ*^{2}-bis-{(*κ*^{2}*S,S*-S$_2$CN(*^{i}Pr*)CH$_2$CONH)$_2$C$_6$H$_4$}] (2b). Brown; MW: 1040.43,Yield: *ca* 0.151 g, 58%; m.p. 256 °C dec.ES-MS: 1042.3 (M+2H). Infrared spectrum (KBr disc,

cm^{-1}): 3472.66s, 3164.43w, 2973.53m, 2882.95w, 2834.41w, 2073.63w, 1758.93m, 1707.82w, 1639.47m, 1604.80w, 1555.96s, 1492.11w, 1412.92vs, 1374.50m, 1304.24m, 1232.12w, 1181.17m, 1128.45w, 1113.51w, 1071.97m, 1019.11m, 967.67w, 927.61w, 813.47w, 781.90w, 747.10w, 690.73w, 645.34w, 621.18w, 525.71w, 429.47s, 413.46sh.

[Zn_2-μ^2-bis-{(κ^2*S,S*-S_2CN(*i Pr*)CH_2CONH)$_2C_6H_4$}] (2c). Pale Yellow; MW: 1044.10,Yield: *ca* 0.107 g, 41 %; m.p. 259 °C dec.ES-MS: 1045.3 (M+H). Infrared spectrum(KBr disc, cm^{-1}): 3448.13s, 3084.65w, 2976.01m, 2886.93m, 2829.97w, 1763.76w, 1692.06s, 1608.79s, 1546.82s, 1490.83s, 1463.43m, 1446.55m, 1396.19vs, 1303.47w, 1226.22m, 1173.44s, 1128.55m, 1072.52s, 1007.15w, 966.36m, 905.26w, 862.09w, 777.12w, 689.01w, 651.92w, 614.46w, 499.60w, 430.61vs. ^{1}H NMR (400 MHz, DMSO-d6): δ (ppm) 10.033(s, 4H, CON*H*); 7.188-6.853 (m, 8H, *Ph*); 5.188 (t, 4H, C*H* of *^{i}Pr*); 4.443 (s, 8H NCH_2CO); 1.185-1.168 (m, 24H, C$H_3$of ^{i}Pr). ^{13}C NMR (400 MHz, DMSO-d_6) δ ppm: 205.7 **(-N^{13}CS_2)**, 165.7 (C=O); 139.9 (*C*-N), 129.1, 115.5, 114.0, 110.6 (*Ph*), 56.2 (*C*Hof^{i}Pr), 51.1(N*C*H_2CO), 20.0, 19.5 (CH_3 of *^{i}Pr*).DEPT-135, (400 MHz, DMSO-d6) : δ ppm 129.42, 124.09, 119.77, 114.2, 110.5 (*Ph*), 56.16(*C*H of *^{i}Pr*); 51.05,48.52 (N*C*H_2CO), 19.96, 19.56 (*C*H_3 of *^{i}Pr*).

[Ni_2-μ^2-bis-{(κ^2*S,S*-S_2CN(*n Bu*)CH_2CONH)$_2C_6H_4$}] (3a). Green MW: 1086.83, Yield: *ca*0.184 g, 68 %; m.p. 272 °C dec.^{1}H NMR (400 MHz, DMSO-d6): δ (ppm) 10.251 (s, 4H, CON*H*);7.234 (brad m, 8H, *Ph*); 4.405 (s, 8H, NCH_2CO); 2.471 (s, 8H, NCH_2 of *^{n}Bu*); 1.526, 1.216 (m, 16H, CH_2 of *^{n}Bu*); 0.825 (s, 12H, CH_3 of *^{n}Bu*).^{13}C NMR (400 MHz, DMSO-d6): δ (ppm) 207.2 **(-N^{13}*C*S_2)**, 164.4 (*C*=O), 139.3 (*C*-N), 129.5, 114.7, 110.5 (*Ph*), 53.2 (N*C*H_2CO), 51.9, 51.1 (N*C*H_2 of *^{n}Bu*), 28.7, 19.7 (*C*H_2 of *^{n}Bu*); 14.0 (*C*H_3 of *^{n}Bu*).

[Cu_2-μ^2-bis-{(κ^2*S,S*-S_2CN(*n Bu*)CH_2CONH)$_2C_6H_4$}] (3b). Brown; MW: 1096.54,Yield: *ca* 0.134 g, 49%; m.p. 245 °C dec.ES-MS: 1097.2 (M+H). Infrared spectrum(KBr disc, cm^{-1}): 3513.84w, 3288.72w, 3145.03w, 3071.29w, 2957.49s, 2930.59m, 2869.04w, 2680.87w, 2485.31w, 1764.33w, 1690.84vs, 1677.75vs, 1608.39s, 1492.87vs, 1439.39m, 1404.50m, 1365.48m, 1300.61m, 1222.73s, 1169.51w, 1115.46m, 1011.04w, 967.05w,

907.66w, 837.25w, 786.06w, 726.77w, 688.68w, 607.33w, 555.75w, 490.15w, 448.45w, 418.47w.

[Zn_2-μ^2-bis-{(κ^2S,S-$S_2CN(^nBu)CH_2CONH)_2C_6H_4$}] (3c). Light yellow; MW: 1100,Yield: *ca*203 mg, 59 %; m.p. >220 °C dec. ES-MS: 1101.4 (M+H). Infrared spectrum(KBr disc, cm^{-1}): 3516.02m, 3269.62w, 3071.38w, 2958.09s, 2869.32w, 2660.32w, 2474.04w, 2360.33w, 1782.68w, 1692.20vs, 1675.80vs, 1608.33vs, 1547.72s, 1485.15vs, 1423.76m, 1399.63m, 1367.51m, 1304.08m, 1213.81s, 1169.46w, 1112.21m, 1010.49m, 969.16w, 935.85w, 876.79w, 784.38m, 689.66w, 624.91w, 537.70w, 494.11w, 446.80w.^{1}H NMR (400 MHz, DMSO-d6): δ (ppm) 10.096(s, 4H, CON*H*); 7.906-6.891(m, 8H, *Ph*);4.649(s, 8H, NCH_2CO); 3.852 (s, 8H, NCH_2 of ^nBu), 1.678, 1.270(s, 16H, CH_2 of ^{n}Bu); 0.893(m, 12H, CH_3 of ^{n}Bu).^{13}C NMR (400 MHz, DMSO-d6): δ (ppm) 206.8 **(-N$^{13}CS_2$)**, 165.91, 164.53 (C=O), 140.9, 139.8, 139.6 (*C*-N); 129.6, 129.4, 114.4, 110.5 (*Ph*); 57.5, 56.7(N*C*H_2CO), 28.8 (N*C*H_2 of ^nBu); 19.9, (*C*H_2 of ^nBu); 14.2(*C*H_3 of ^nBu).

4.2.5 *In vitro* cytotoxic study

4.2.5.1 Cell line and culture

The hepatomacancer cell line HEP G2 was procured from the National Centre for Cell Science, Pune whereas Dulbecco's Modified Eagle's Medium (DMEM), Fetal Bovine Serum (FBS) and antimycotic–antibiotic solution were procured from Gibco, Invitrogen and Cisplatin from Sigma Aldrich. The cell line was maintained in DMEM with 10% FBS in humidified atmosphere supplied with 5% CO_2 at 37°C and was utilized to examine the cytotoxic activity of testing compounds at varying concentration.

4.2.5.2 MTT assay for cell viability/ proliferation

The MTT assay was used to determine cell growth inhibition. All the compounds viz. L',L^1, L^2, L^3 and their ensuing transition metal dithiocarbamate complexes 1a-1c, 2a-2c, 3a-3b were dissolved in 5% DMSO and then diluted with culture media. Cells were seeded in 96-well plates at a density of 1×10^3 cells per well and incubated for 24hrs after

which they were treated with different concentrations (6.25µg/ml, 12.5µg/ml, 25µg/ml, 50µg/ml and 100 µg/ml) of compounds for 24hrs. Under the similar experimental conditions cisplatin was also screened against HepG2 at different doses. Finally the media was removed and the cells were incubated with 10µL of 5 mg/ml stock solution of MTT in PBS for 4hrs at 37°C in 5% CO_2 incubator. The resultant formazan crystal formed by metabolically viable cells was dissolved by adding DMSO. The optical density was measured at 540nm by an ELISA reader (BIOTEK ELX800 Universal Microplate Reader).

4.2.5.3 Statistical Analysis for Determination of IC_{50}

Data obtained was analyzed in Prism/OriginPro 8 for standard error and probit analysis. The percent cytotoxicity index (% CI) was calculated as follows:

% CI= [1− (OD of treated cells/ OD of control cells)] × 100 %

Where, CI= cytotoxicity index, OD = optical density.

A plot of % CI versus concentration was obtained from the experimental data for each set of experiments. The values of IC_{50} (50% growth inhibition of cell) were determined from the graph.

4.2.5.4 Assessment of apoptosis AO/EtBr staining

Cells were grown in 24 well-plate (5 x 10^5) and were incubated in a CO_2 incubator at 37^0C. Cells were dosed with IC50 concentration of compounds. After 24hrs of incubation, cells were washed with PBS and stained with 200µl of AO-EtBr mixture (100µg/ml AO: 100µg/ml EtBr). Cells were observed under FLoid™ Cell Imaging Station (Life Technologies) fluorescent microscope at 20X magnification.

4.3 Result and Discussion

4.3.1 Syntheses and characterization

α-chloro amide precursor 1,3-bis(2-chloroacetamido)phenylene **L'** was synthesized by a modified literature procedures [22] and this modification was scalable to 91 % in less time, unlike the original method (Scheme 1) and it was characterized prior to its use.The unambiguous molecular structure of **L'** was further determined by single crystal X-ray diffraction study. The structural description of this molecule displaying an unusual halogen bonding interactions is elaborated in latter stage.

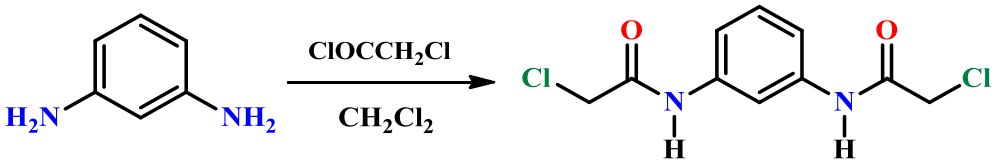

Scheme 1: Preparation of 1,3-bis(2-chloroacetamido)phenylene (**L'**)

Nucleophilic substitution of α-chlorosubstituent**L'** with different primary amines efficiently yielded a new series of diamine derivatives such as 1,3-bis(2-(cyclohexylamino)acetamido)phenylene (**L**^{1}), 1,3-bis(2-(isopropylamino)acetamido)phenylene (**L**^{2}) and 1,3-bis(2-(n-butylamino)acetamido) phenylene (**L**^{3}) in >80 % yields. (Scheme 2). L^{1}-L^{3}have been characterized suitably by standard spectroscopic methods prior to their use.

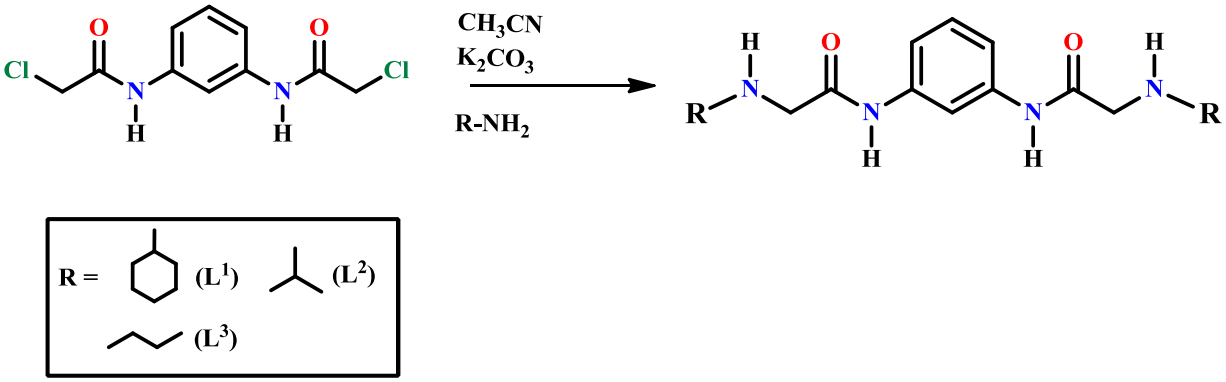

Scheme 2: Synthesis of 1,3-bis(alkylamino)acetamido)phenylenes **L**^{1}-**L**^{3}.

Coordination driven self-assembly process involving corresponding diamine**L^1-L^3** with CS_2 and transition metal ion viz. Ni^{II}, Cu^{II} or Zn^{II} at room temperature affords access to a new series of bimetallic dithiocarbamate macrocyclic compounds **1a-1c, 2a-2c, 3a-3c** in good yields. The synthetic procedure is illustrated in **Scheme 3**. Previously, Professor Beers *el.al* [23] have used a number of diamino derivatives of o-phenylenediamine m-o-phenylenediamine to derive transition metal dithiocarbamate macrocyclic compounds and explored their supramolecular chemistry. The affluence of synthesis and their potentials to be substantial cytotoxicagents would further supplement the worth of the current series of bimetallic macrocyclic complexes. Although the newly synthesized compounds, **L^1-L^3** and bimetallic complexes **1a-1c, 2a-2c, 3a-3c** could not be obtained in the crystalline state, the composition and structures of **L^1-L^3**, **1a-1c**, **2a-2c** and **3a-3c**were confirmed by standard spectroscopic (IR, Mass, ^{1}H, ^{13}C, DEPT 135, ^{1}H DOSY NMR and UV-visible) and thermogravimetric data. Further a DFT level calculation has been performed on representative compounds to reinforce the experimental data.

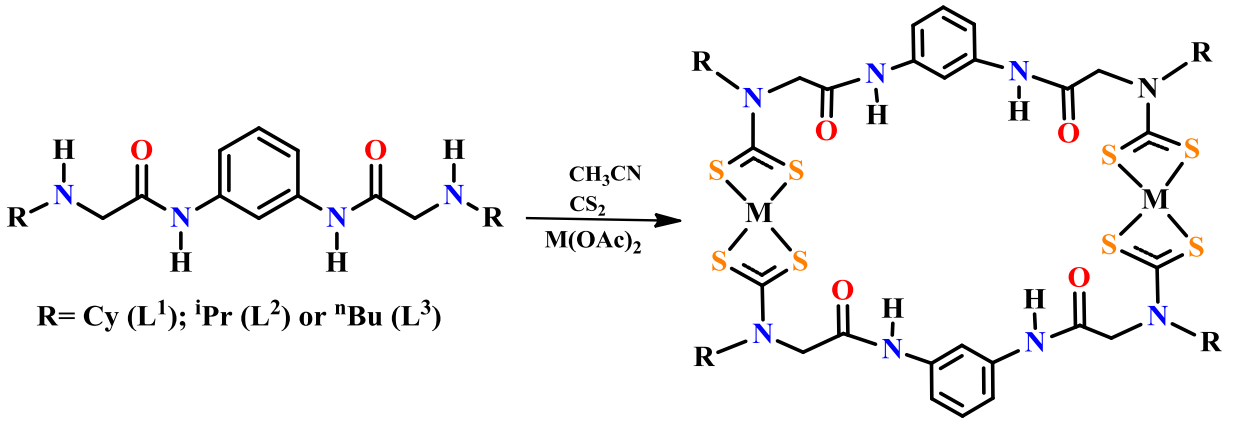

R= Cy (L^1); ^{i}Pr (L^2) or ^{n}Bu (L^3)

R= Cy; M = Ni^{II} (1a), Cu^{II} (1b), Zn^{II} (1c)
R = ^{i}Pr; M = Ni^{II} (2a), Cu^{II} (2b), Zn^{II} (2c)
R= ^{n}Bu; M = Ni^{II} (3a), Cu^{II} (3b), Zn^{II} (3c)

Scheme 3: Coordination driven self-assembly process affording binuclear metallomacrocyclic compounds **1a-1c**, **2a-2c** and **3a-3c**.

4.3.2 NMR , Mass and IR spectral study

The ^{1}H NMR spectra of diamine derivatives **L^1-L^3** displayed most characteristic signals in the region of 2.49-1.85 ppm, 2.74-2.32 ppm 3.40-3.34/1.98 ppm and 9.90-9.81 due to amine (–NH), methine (-N*CH*),methylene (-N*CH*$_2$CO/-NCH$_2$) and amide (-CON*H*) groups respectively which are consistent with the literature.^{1}H NMR signals corresponding to the protons of aromatic and *N*-alkyl substituents appeared as multiplets due to coupling with adjacent protons. The ^{13}C NMR spectra for **L^1-L^3** gave characteristic signals in the range of 172 -171 ppm, 56-51 ppm and 50.7-48.6 ppm are attributed to the carbonyl carbons, the α-methylene carbons (N*C*H$_2$CO) and aliphatic *N*-substituents (N*C*H/ N*C*H$_2$) respectively which are further supported by and DEPT-135 study (Annexure 19-27). The mass spectra of **L^1-L^3** gave molecular ion peaks at 386.1, 307.2 and 335.2 attributable to [M$^+$] or [M+H] molecular ions respectively as shown in (Annexure 1-3). In the IR spectra of **L^1-L^3**, the characteristic band observed in 3400–3500 cm^{-1}range is diagnostic of υ(N-H) stretching vibration. The broad or multiple nature of υ(N-H) vibrations suggests the possibility of involvement of amide/amine functionalities in the intermolecular hydrogen bonding in the solid state. The weak intensity bands appeared in the regions of 3087-2926 cm^{-1} are attributable to the aromatic υ(C-H) stretching vibrations, whereas bands appeared in the regions of 875-827 cm^{-1} are assignable to the aromatic υ(C-H) out-of plane bending vibrations, a characteristic feature of phenyl ring. [24] Furthermore, **L^1-L^3** display strong bands (1652–1690 cm^{-1}) and medium intensity bands (1186-1129 cm^{-1}) due to υ(C=O) and υ(C-N) vibrations (Annexure 12-14).[25]

The diamagnetic Ni^{II} (**1a, 2a** and **3a**) and Zn^{II} (**1c, 2c** and **3c**) complexes showed disappearance of amine (–NH) signal and substantial down-field shift of methine (-N*CH*), methylene (-N*CH*$_2$CO/-NCH$_2$) and amide (-CON*H*) signals, compared to their positions in the ^{1}H NMR spectra of respective diamino precursors. Importantly, the ^{13}C NMR spectra of these complexes displayed a very downfield signals in the range of 204.1–207.2 ppm and confirms the presence of coordinated dithiocarbamate (**-N^{13}CS$_2$**) moieties (Annexure 28-38). These observations ascertained the formation of these complexes. Literature suggests that the metal-directed self-assembly of a discrete molecular structure depends on the formation of these bimetallic dithiocarbamate macrocyclic complexes

apparently profited from stereo-electronic features of ligand framework,[26]metal centers [27] as well as thermodynamic conditions. [28] Furthermore, ^{1}H DOSY NMR spectrum of complex **1a** (Fig. 1), **2a** (Annexure 34) and **2c** (Annexure 38) unambiguously display the presence of only one type of species in solution and ruled out the possibility of mixture of oligomer/polymer.

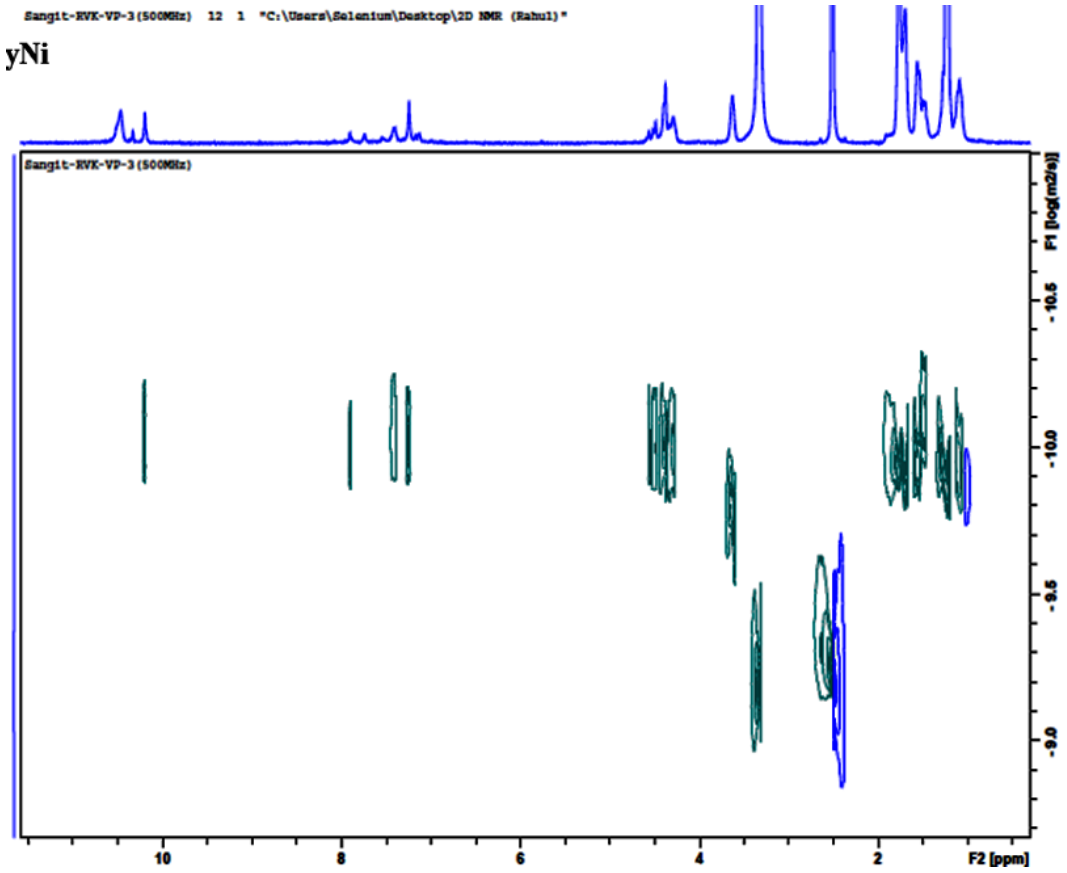

Fig. 1: ^{1}H DOSY NMR spectrum of **(1a)**

The ESI-MS spectra of these complexes gave molecular ion peaks which are either corresponding to [M+H], [M+2H] or [M^{+}] along with expected molecular fragments. The FT IR spectra of all the complexes displayed characteristic IR bands in the range of 1492–1404 cm^{-1} and 1051-1007 cm^{-1} due to ν(N-CSS) and ν_{as}(CSS) stretching vibrations, suggestive of an anisobidentate chelation of the dithiocarbamate ligand moieties in these complexes.[25, 30] These spectral data are in accord with the literature and clearly supports the formation of complexes.[25,29, 30]

4.3.3 UV-visible absorption, magnetic moment and florescence emission study

Similar to other diamino precursor [25] **L^1-L^3** exhibit a single prominent absorption band at ~300 nm which are attributable to π→π* (phenyl) transitions. However, bimetallic dithiocarbamatemacrocyclic compounds **1a-1c, 2a-2c,** and **3a-3c** show two principal bands in the range of 300-323 nm and 352-438 nm attributable to π→π* (phenyl) and charge transfer transitions, respectively as shown in Fig. 2, (Annexure 39) and (Annexure 40) Besides, copper complexes **1b, 2b** and **3b** display additional band at in the region of 633-639 nm which is attributable to to *d-d* transition. Overall, the absorption behavior of these compounds are consistent with the literature.[25, 30, 31] The magnetic data along with UV-visible absorption bands (Table 1) suggest a distorted square planar environment around Ni(II)/ Cu(II) and distorted tetrahedral environment around Zn(II) in their respective bimetallic dithiocarbamate complexes.

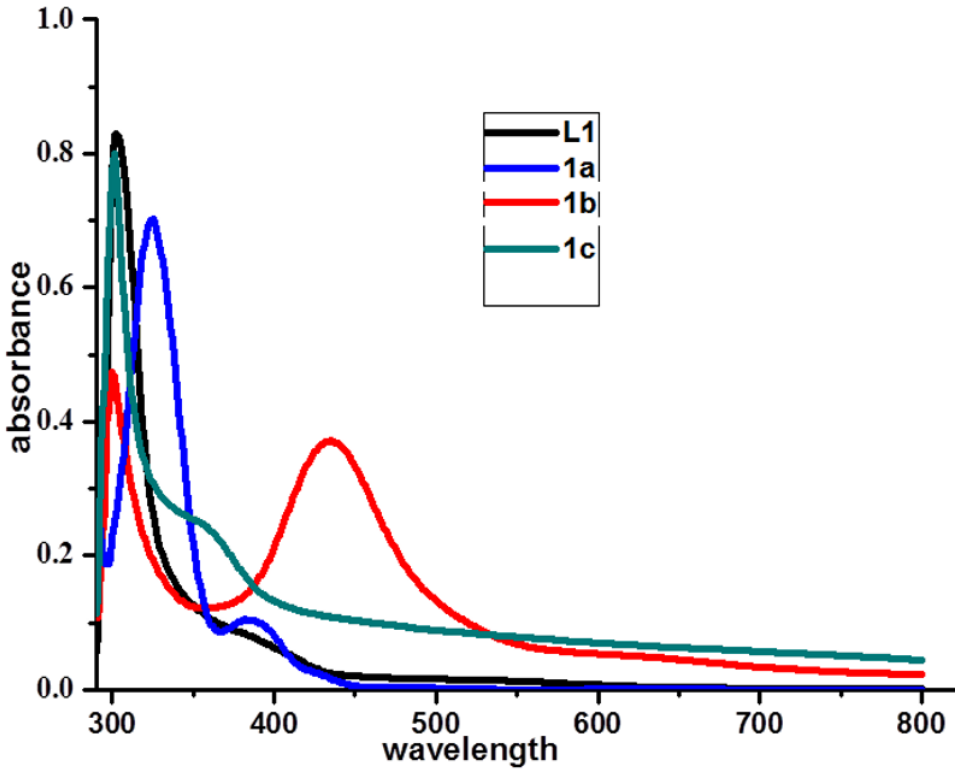

Figure. 2: UV–visible absorption spectra of compounds **L^1** and **1a, 1b, 1c** in DMSO solution.

Interestingly, all the ligand precursors $\mathbf{L^1}$-$\mathbf{L^3}$ fluoresces well in the region of 326-344 nm from locally excited π→π* transition states, however fluorescence property of these diamines has been substantially quenched upon the formation of respective binuclear dithiocarbamate macrocyclic complexes with Ni(II), Cu(II) or Zn(II) (Annexure 41-43). Although zinc ions are known to simulate the fluorescence properties of transition metal dithiocarbamate complexes.[24b] however this unusual fluorescence quenching behavior of zinc ions is consistent with our earlier observation. [25]

Table 1

UV-visible absorption, magnetic moment and fluorescence data for the compounds

Entry	UV-visible spectral data (10^{-3} M DMF)	Wave number	Magnetic Moment μ_{eff}(BM)	Fluorescence spectral data (10^{-3} M DMF)	
	λ_{max} nm (ε L $Mol^{-1}cm^{-1}$)			λ_{ex} nm	λ_{em}(nm) (Intensity)
L^1	303(827.1)π→π*	3300	-	303	344 (291) π*→π
L^2	300 (592.7) π→π*	3333	-	300	340(277)
L^3	298 (490.2)π→π*	3355	-	298	326(127) π*→π
1a	324(42319) π→π* 387 (6204.8) n→π*	3086 2583	dia	324	Non fluorescent
1b	300(1576.6) π→π* 435(1235.6) charge transfer 639(159.66) *d-d transition*	3333 2298 1564	1.80	300	Non fluorescent
1c	300 (7992)π→π* 360 (2398)π→π*	3333 2777	dia	300	330(17), π*→π
2a	324 (69700) π→π* 390 (11370)n→π*	3086 2564	dia	324	Non Fluorescent
2b	301 (6644) π→π* 434 (7714) charge transfer 633 (552) *d-d transition*	3322 2304 1579	1.81	301	331(29), π*→π
2c	301 (6875) π→π* 352 (1584) n→π*	3322 2840	dia	301	331(11), π*→π
3a	323 (49343) π→π* 390 (8969) n→π*	3095 2564		323	Non Fluorescent
3b	300 (4975) π→π* 438 (4951) charge transfer 638 (392) *d-d transition*	3333 2283 1567	1.84	300	328(61) π*→π
3c	300 (10512) π→π* 415 (2486) charge transfer	3333 2427	dia	300	328(58) π*→π

4.3.4 TGA/DTA study

The thermogravimetric study was performed on $\mathbf{L^1}$, $\mathbf{L^3}$ and bimetallic dithiocarbamatemacrocyclic complexes **1a-1b, 2a-2c** and **3a-3b** in the temperature ranges from room temperature to 550 ºC. The heating rate was suitably controlled at 10 ºC min^{-1} under nitrogen atmosphere. The stable residual mass obtained for each compounds along with temperature ranges corresponding to percentage weight loss during the decomposition and variable rate of decompositions observed on DTG curves are similar to other transition metal dithiocarbamate complexes, [25,30-31] a multistage mass loss on corresponding DTG curves and DTA peaks due to endothermic and/or exothermic elimination of molecular fragments can be clearly seen on thermogravimetric plots for these compounds. Notably, thermal decompositions of all the complexes start before their melting points. Complexes **2c** and **3a** exhibit 47.8 % and 40.7 % of degradations on TG curves respectively whereas complex **1a** displayed maximum degradation of 70 % of TG curve. None of the complexes gave a stable residual mass up to 550 ºC.

4.3.5 Geometry Optimization

It was relevant to accomplish full geometry optimization of diamine precursor $\mathbf{L^1}$ and its transition metal dithiocarbamate complexes **1a-1c** (Fig. 3) for a better understanding of the spectroscopic results. All the calculations have been performed by using density functional theory (DFT) at B3LYP/6-31G (d, p) and B3LYP/LanL2DZ basis sets, respectively. The structural parameters *viz* bond lengths and bond angles obtained theoretically were suitably compared with the X-ray data of closely related compounds (Table 2) [32] and found in good agreement. In recent time, our group [10b,33] has been successfully used DFT calculations to reproduce the geometries obtained by X-ray diffraction analysis. The trans annular M···M distances of 32 membered macrocycles **1a-1c** fall in the expected range when compared with the similar distances calculated for analogues systems. [25,30]

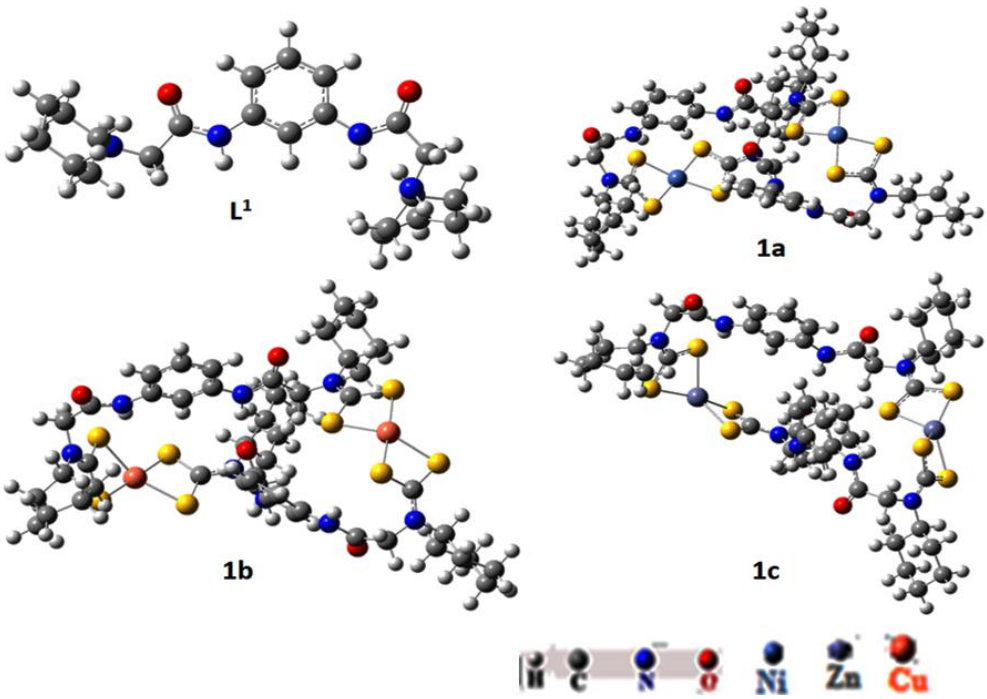

Fig. 3: Optimized geometry for the minimum energy conformation for $\mathbf{L^1}$, its dithiocarbamate salt $\mathbf{L^1}$**-dtc** and complexes **1a-1c**.

Table 2
X-ray crystallographically obtained bond lengths (Å) and bond angles (°) for analogues Ni^{II} based dithiocarbamate macrocycle, [32a] Cu^{II} based dithiocarbamate macrocycle,[32b] Zn^{II} based dithiocarbamatemacrocycle [32c] and computed values for complexes **1a**, **1b** and **1c**.

Parametres	$\mathbf{1a^x}$	$\mathbf{1b^x}$	$\mathbf{1c^x}$
N—C	1.28 -1.50[32a] 1.33-1.34	1.318-1.328[32b] 1.33-1.34	1.333-1.363[32c] 1.340-1.348
C—S	1.69-1.74[32a] 1.73-1.74	1.719-1.727[32b] 1.73-1.75	1.717-1.782[32c] 1.73-1.76
M—S	2.16-2.22[32a] 2.25-2.29	2.288-2.301[32b] 2.38-2.42	2.32-2.44[32c] 2.41-2.47
Transannular M-M	11.852	11.77	11.80
S—M—S (chelate)	78.99-79.87[32a] 77.0-78.5	77.59[32b] 74.9-75.6	79.5-81.2[32c] 74.8-76.2
S—M—S	100.31-177.14[32a] 100.1-101.8	101.72-103.48[32b] 102.3-108.6	126.53-136.00 [32c] 110.7-131.6

[x]Computed values for the metallomacrocycles **1a**, **1b** and **1c** are shown beneath the experimental observed values.

In **1a-1c**, two ligand molecules bridges over two metal centers and each of the metal ions Ni(II), Cu(II) or Zn(II) are bonded through available chelating sites of terminal dithiocarbamate moieties resulted into the formation of binuclear dithiocarbamate macrocyclic compounds. The angles between the two S−M−S planes deviate substantially from coplanarity and the S−M−S angles involving trans S-atoms differ largely from 180° in the molecules of **1a-1b**. The geometry around the metal ions in these complexes is thus essentially distorted square planar. However, a close deviation of similar angle from 180° in the molecule of **1c** ascertained the distorted tetrahedral geometry around Zn(II) ion. Further it appears that M–S bond lengths around one metal center in a particular complex *ca* binuclear Ni(II) dithiocarbamate complex **1a** is comparable with the similar distances around other metal center whereas these distances deviate significantly in the binuclear Cu(II) complex **1b** and Zn(II) complex **1c** (Table 2). Moreover, the λ_{max} values obtained by computational study are comparable with the λ_{max} values determined experimentally by means of UV-visible absorptions which further validate the computational investigations. Unlike our earlier observation [25] all four *N*-Cy substituents in **1a-1c** are projected outwards of the 32-member molecular cavity which can be visualized in the optimized geometry (Fig. 3) and in the spacefilled model. It may be noted that all the amide groups are projected outward while sulfurs of dithiocarbamate are inclined inward in these macrocyclic compounds, making the macrocyclic cavity hydrophobic. Molecular electrostatic surface potentials of any chemical species, [34] has appeared to be a crucial factor for prediction of the properties and potential sites for reactivity in biological systems. The MESP of complexes **1a-1c** (Fig. 4) clearly indicate the presence of slight negative potential around amide oxygen and positive potential around amide proton (Red and blue colourin MESP images symbolizes localization of negative and positive potential respectively). This provides a number of donor-acceptor sites and enables these metallomacrocyclic compounds for effective interactions with biomolecules, resulting into the increased concentration of complexes at the site of action through effective cellular membrane transportation. Probably due to these added features of current series of metallomacrocycles, their potentials to be effective cytotoxic agents are significantly enhanced (discussed latter).

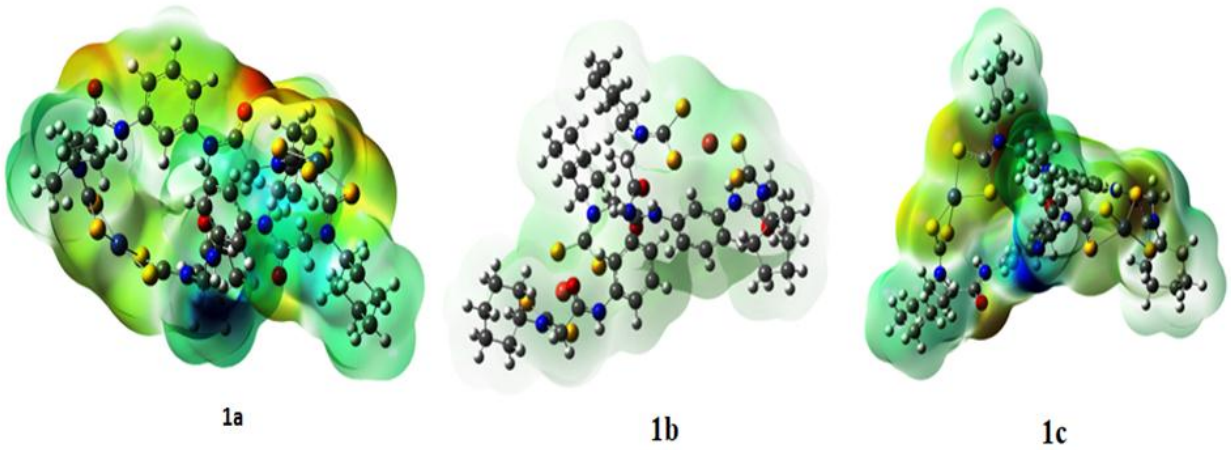

Fig. 4: Representations of electron density from total SCF density (Isovalue= 0.0004; mapped with ESP).

4.3.6 Structural description of L'

The crystal data and structure refinement for **L'** are given in Table 2. Molecule crystallizes in non-centrosymmetric monoclinic Cc space group. The X-ray crystal structure of **L'** shows the asymmetric unit contains full molecule of [$C_{10}H_{10}Cl_2N_2O_2$] as shown in Fig. 5(a).There are four such units in the unit cell. The selected bond distance (Å) and bond angle (°) for **L'** are: C(1)-Cl(1) 1.772(7), Cl(2)-C(10) 1.749(6), C(9)-N(2) 1.332(6), C(9)-O(2) 1.223(6), C(7)-N(2) 1.413(7), C(9)-C(10) 1.527(7), C(2)-N(1) 1.337(8), C(3)-N(1) 1.417(6), C(1)-C(2) 1.519(8), C(2)-O(1) 1.191(7) and Cl(1)-C(1)-C(2) 109.9(5), C(1)-C(2)-N(1) 113.6(5), C(2)-N(1)-C(3) 125.8(4), C(1)-C(2)-O(1) 122.6(6), N(1)-C(3)-C(8) 117.1(4), Cl(2)-C(10)-C(9) 113.0(4), C(10)-C(9)-N(2) 112.5(4), C(9)-N(2)-C(7) 127.4(4), C(10)-C(9)-O(2) 121.9(5), N(2)-C(7)-C(8) 123.1(4), respectively. The structural parameters are found to be in the normal range [33,35] and require no further comments. Interestingly, molecules of **L'** showed propensity of formation of an unusual [36] C-Cl…π intermolecular donor-acceptor interactions (Fig. 5(b) along with C-H…Cl, CH...O and N-H...O donor-acceptor interactions. The significant intermolecular interactions such as interatomic distances (Å) and bond angles (°) found in compound **L'** are provided in Table 3.

Table 3.Crystallographic data and structure refinement parameters for **L'**.

Empirical formula	$C_{10}H_{10}Cl_2N_2O_2$
Formula weight	261.10
Crystal system	monoclinic
Space group	Cc
a (Å)	4.79673(19)
b (Å)	26.6576(13)
c (Å)	9.1390(4)
α (°)	90
β (°)	100.720(4)
γ (°)	90
V (Å^3), Z	1148.20(9), 4
Calculated density (g cm-3)	1.510
Absorption coefficient (mm^{-1})	4.995
F(000)	536.0
2θ range for data collection (°)	6.632-151.278
Index ranges	– 4<=h<=5,– 32<=k<=31,– 11<=l<=11
Reflections collected/ unique	4080
Independent reflections	1514 [R_{int} = 0.0432]
Data / restraints / parameters	1514 / 2 / 145
Goodness-of-fit on F^2	1.090
Final R indices [I>2σ (I)]	R1 = 0.0557, wR2 = 0.1604
R indices (all data)	R1 = 0.0569, wR2 = 0.1640
Largest diff. peak/ hole (e A^{-3})	0.53/ – 0.25

Table 4 Significant intermolecular interactions [Interatomic distances (Å), and bond angles (°)] found in compound **L'**

Compound	D─H…A	D─H	H…A	D…A	<DHA (β)	<α
L'	C_1─ Cl_1… $C_{g1'}$ [$C_{g1'}$**:** $C_3C_4C_5C_6C_7C_8$]	1.772	3.876	5.529	154.56	7.88
	C_1─H_{1B}…O_1	0.970	2.602	3.397		
	N_1─H_1…O_1	0.860	1.970	2.830		
	C_2─O_1…H_{1B}	1.191	2.602	3.543		
	C_2─O_1…H_1	1.191	1.970	3.153		
	C_9─O_2…H_2	1.224	2.041	3.095		
	C_{10}─Cl_2…H_6	1.749	2.922	4.527		
	N_2─H_2…O_2	0.860	2.041	2.859		
	C_6─H_6…Cl_2	0.930	2.922	3.688		

Notably, C(2)-O(1) group of asymmetric molecule is involved in the bifurcated hydrogen bonding interactions with the adjacent molecule by involving N(1)-H(1) and C(1)-H(1B) and arranging the incoming molecule parallel along a-axis. However C(9)-O(2) group of asymmetric molecule is connecting the third molecule via interaction with N(2)-H(2)

group and arranging this molecules orthogonally along a-axis. Interestingly C(1)-Cl(1) group and the centroid of the phenyl group (Cg1: $C_3C_4C_5C_6C_7C_8$) of the asymmetric molecule is involved in C(1)-Cl(1)...π donor–acceptor interactions, respectively, arranging the neighbouring two molecules parallel along c-axis. According to the statistical data retrieved from PDB for a majority of protein–ligand complexes, [37] the *α* angle (angles between the vector along the Cg–Cl line and the normal to the plane of the ring) and the *β* angle (∠ C–Cl–Cg º) varies in the range of 20-30 º and 160-180 º, respectively. Compound L' display Cl...Cg distance (3.876 Å) and favourable α angle (7.88°) in the standard range [37-38]. The α angle was calculated from α = 90°-θ where θ is the angle of intersection of the phenyl ring plane (82.12°) and the β angle C9-Cl1···Cg (Cg: $C_3C_4C_5C_6C_7C_8$) of 154.56° is sufficiently large to expedite the effective C–Cl...π interactions.(Table. 4) The remaining groups in the molecule viz. $C(10)_{phenyl}$-H(6) and C(10)-Cl(2) are involved in C-H…Cl donor-acceptor interactions and arranging two neighbouring molecules orthogonally along a-axis. In solid state, the molecule present in the asymmetric unit forms eight donor-acceptor contacts that lead to supramolecular aggregate consists of nine molecules as shown in Fig.5(c). Notably, C-Cl...π donor-acceptor interactions efficiently managed the growth of self-assembly along *c*-axis, however, the dimensionality has been extended along *a*-axis through C-H...O, N-H...O and C-H…Cl interactions leading to the fascinating 2D infinite supramolecular molecular sheet like architecture as shown in Fig.5(d).

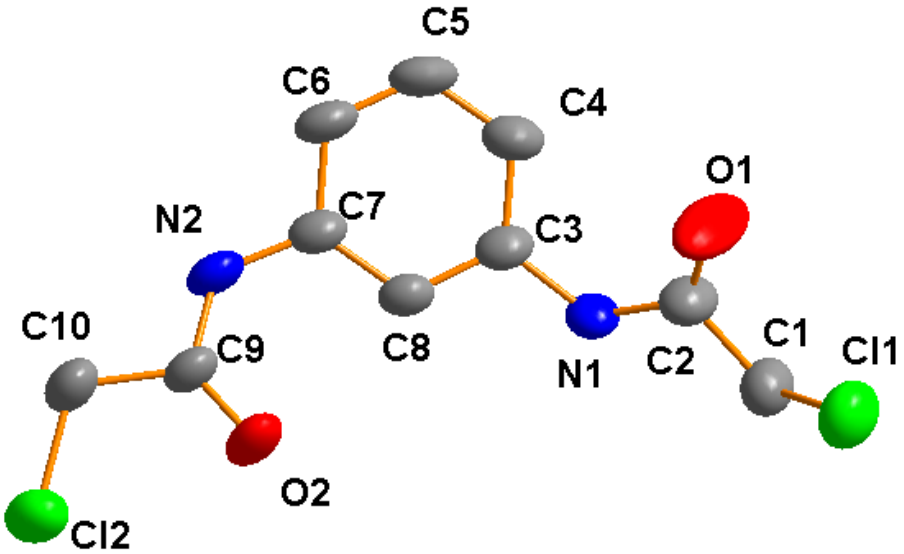

(a)

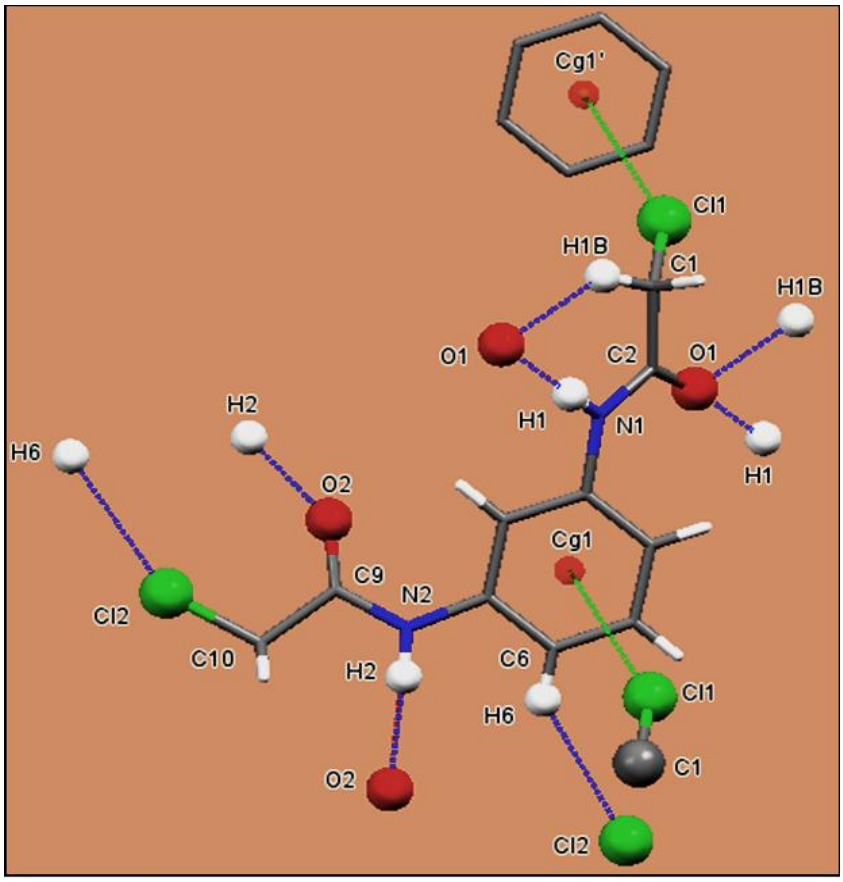
Cg1'
Cl1
H1B
C1
H1B
O1
C2
O1
H2
H1
N1
H6
O2
H1
Cg1
C9
N2
Cl2
C10
H2
C6
Cl1
H6
C1
O2
Cl2

(b)

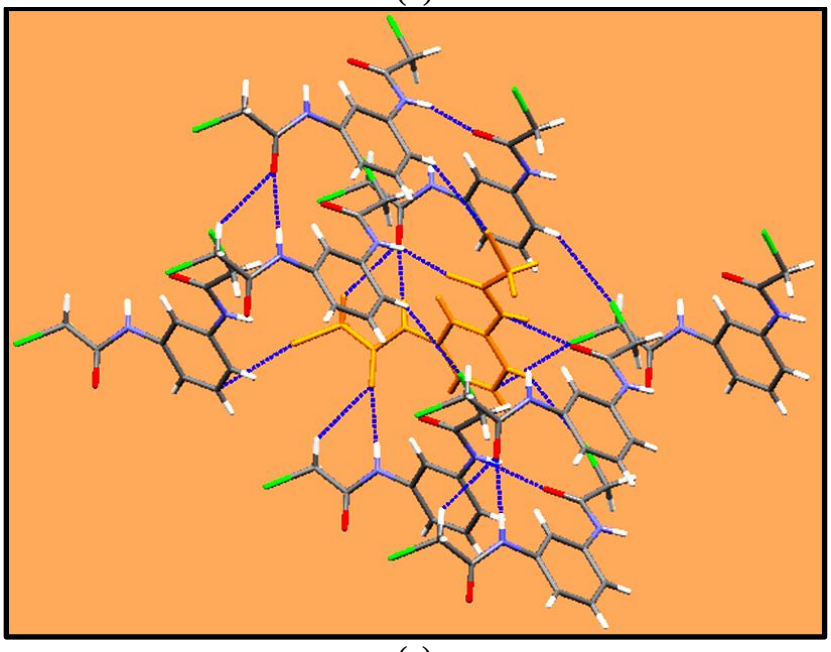

(c)

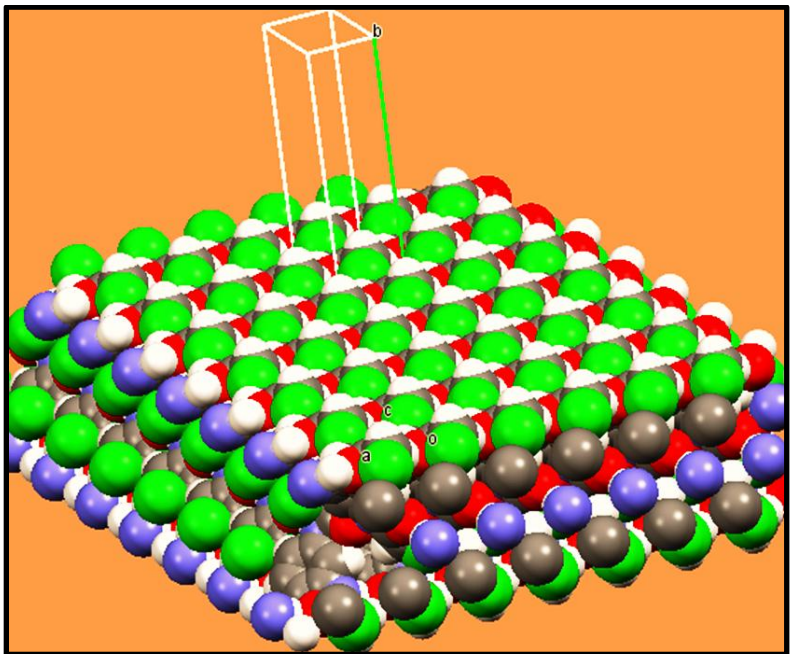

(d)

Fig. 5: (a) X-ray structure of compound **L'**; (b) Propensity of formation of intermolecular contacts in molecules of **L'**; (c) Supramolecular unit consists of nine molecule aggregates involving CCl...π, CH...Cl, CH...O and NH…O donor-acceptor interactions; (d) View of molecular packing in spacefill model exposing formation of 2D infinite supramolecular sheet like architecture.

It may be noted that the additional data on C-Cl…π contacts would certainly help us to ascertain the biological and structural importance of synthetic molecules as protein data bank (PDB) suggests the availability of only limited number of C-Cl…π interactions in crystal structures of protein–ligand complexes.[37] The hydrogen bonds and stacking interactions like C–H…O,[39] N–H…O,[40] C–H…π.[41] and π…π[42] interactions are being considered as main directing tool in the organization of molecules in both chemistry as well as in biology and therefore any step taken into predictable molecular packing is a practical movement. The enhanced cytotoxicity of α-chloroamide *ca* 1, 3-bis(2-chloroacetamido)phenylene **L' (**discussed latter**)** and others[10a,25] compared to their diamino derivatives is apparently associated with their ability to form halogen bonding interactions.

4.3.7 *In vitro* cytotoxic activity

MTT assay was carried out to study the *in vitro*cytotoxic behavior of all the synthesized compounds against human hepatocellular carcinoma cell line Hep G2 (Hepatoma). Liver metababolsim and xenobiotics toxicity [43] are largely studied through the selection of HepG2 cell line. Various significant processes of drug metabolism and modification of toxic substances are chiefly looked after by the hepatocytes. All these observations along with the very few reports on the biological perspective of m-phenylene diamine led us to study the cytotoxic potential of all the newly synthesized compounds by MTT assay against the malignant tumor cell line HepG2 (Hepatoma). The cytotoxicity observed for these compounds were equated with the standard drug cisplatin [C]. The 50% inhibition concentration (IC_{50}) values obtained after incubation for 24hrs for all the compounds against said cell lines are abridged in Table. 5 and Figure. 6. Further, compounds displaying IC_{50} lower than Cisplatin (**L', L^1, 1a, 1b, 1c, 2a, 2b, 2c, L^3,3a, 3b, 3c**) were tested on normal liver cell line (WRL-68) under similar conditions to understand the specificity of these compounds.

Table. 5: IC_{50} values for entry1-15 against Hep G2 and WRL-68 cell lines.

Entry	Compounds	HepG2 IC50 (μM)	WRL-68 IC50 (μM)
1	m-phenylene diamine **L**	272.88 ± 0.16	-
2	1, 3-bis(2-chloroacetamido)phenylene **L'**	12.67 ± 0.08	474.53 ± 0.48
3	1,3-bis(2-(cyclohexylamino)acetamido)phenylene $\mathbf{L^1}$	65.07 ± 0.26	403.16 ± 0.48
4	$[Ni_2$-μ^2-bis-$\{(\kappa^2S,S$-$S_2CN(Cy)CH_2CONH)_2C_6H_4\}]$ **1a**	20.14 ± 0.50	96.31 ± 0.72
5	$[Cu_2$-μ^2-bis-$\{(\kappa^2S,S$-$S_2CN(Cy)CH_2CONH)_2C_6H_4\}]$ **1b**	36.35 ± 0.52	130.27 ± 0.33
6	$[Zn_2$-μ^2-bis-$\{(\kappa^2S,S$-$S_2CN(Cy)CH_2CONH)_2C_6H_4\}]$ **1c**	13.78 ± 0.50	66.67 ± 0.48
7	1, 3-bis(2-(isopropylamino)acetamido)phenylene $\mathbf{L^2}$	90 ± 0.44	-
8	$[Ni_2$-μ^2-bis-$\{(\kappa^2S,S$-$S_2CN(^iPr)CH_2CONH)_2C_6H_4\}]$ **2a**	11.40 ± 0.32	110.44 ± 0.82
9	$[Cu_2$-μ^2-bis-$\{(\kappa^2S,S$-$S_2CN(^iPr)CH_2CONH)_2C_6H_4\}]$ **2b**	20.07 ± 0.37	140.23 ± 0.31
10	$[Zn_2$-μ^2-bis-$\{(\kappa^2S,S$-$S_2CN(^iPr)CH_2CONH)_2C_6H_4\}]$ **2c**	4.80 ± 0.42	116.19 ± 0.52
11	1, 3-bis(2-(n-butylamino)acetamido)phenylene $\mathbf{L^3}$	16.82 ± 0.35	292.90 ± 0.62
12	$[Ni_2$-μ^2-bis-$\{(\kappa^2S,S$-$S_2CN(^nBu)CH_2CONH)_2C_6H_4\}]$ **3a**	9.86 ± 0.45	95.70 ± 0.53
13	$[Cu_2$-μ^2-bis-$\{(\kappa^2S,S$-$S_2CN(^nBu)CH_2CONH)_2C_6H_4\}]$**3b**	20.90 ± 0.40	72.65 ± 0.24
14	$[Zn_2$-μ^2-bis-$\{(\kappa^2S,S$-$S_2CN(^nBu)CH_2CONH)_2C_6H_4\}]$**3c**	6.73 ± 0.44	83.50 ± 0.48
Cisplatin	**C**	75.67 ± 0.33	266.67 ± 0.33

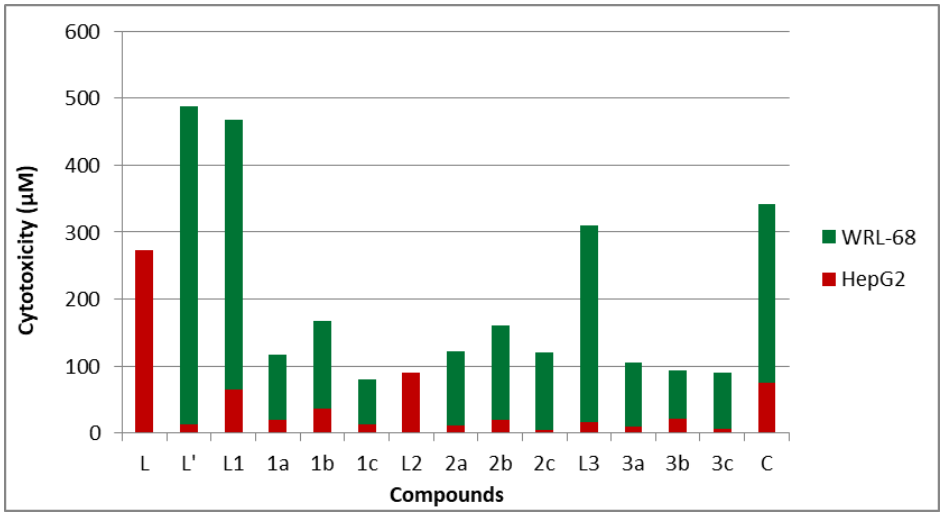

Fig. 6: Cytotoxic activity IC_{50} values (µM) for **L** and its derivatives **L'**, **1a-1c**, **2a-2c** and **3a-3c**.

The results clearly suggest that all the compounds (except $\mathbf{L^2}$) exhibited excellent cytotoxic activity compared to the reference drug cisplatin and specificity for cancer cells over normal liver cells (Fig. 6, Table 5). Compound **2c** shows almost 15 fold better cytotoxic activity against Hep G2 cell line (4.80 ± 0.42 µM), compared to the reference drug Cisplatin (75.67 ± 0.33 µM) whereas **3a** and **3c** exhibited 7-11 fold better activity. It is observed that the activity of the first derivative of m-phenylenediamine **L'** (12.67 ± 0.08 µM**)** could not upheld on further modification to $\mathbf{L^1}$ (65.07 ± 0.26 µM) and $\mathbf{L^3}$ (16.82 ± 0.35 µM**),** however the activity of these is still superior than cisplatin**.** On further derivatization of $\mathbf{L^1}$-$\mathbf{L^3}$ the cytotoxic potentials of their corresponding bimetallic dithiocarbamate complexes **1a-1c, 2a-2c, 3a-3c** evidently improves tremendously. Compound **2c** shows almost 15 fold better cytotoxic activity, however **1c (**13.78 ± 0.50 µM**)** and **2a (**11.40 ± 0.32 µM**)** exhibit 5-6 fold. **1a** (20.14 ± 0.50µM), **1b** (36.35 ± 0.52µM), **2b** (20.07 ± 0.37µM) and **3b** (20.90 ± 0.40µM) exhibit 3-2 fold improved cytotoxic activity than the reference drug cispaltin.

Oncological research highly emphases on genes and signals regulating apoptosis. Apoptosis is a genetically regulated programmed cell death that manages the development of multicellular organisms by maintaining cell populations in tissues, aging and regulating immune system. The shrinking of cells, a distinguishing apoptotic sign,[44]

indicating the initiation of apoptosis as part of the mechanism of action of these compounds can be clearly pictured by acridine orange/ethidium bromide (AO/EB) staining (Fig. 7) which marks nuclear changes and differentiates between viable, apoptotic and necrotic cells. Most of the compounds were stained for AO/EB wherein viable cells are marked by AO and show green fluorescence whereas apoptotic cells are stained by EB and show orange to red fluorescence with condensed chromatin. [45]

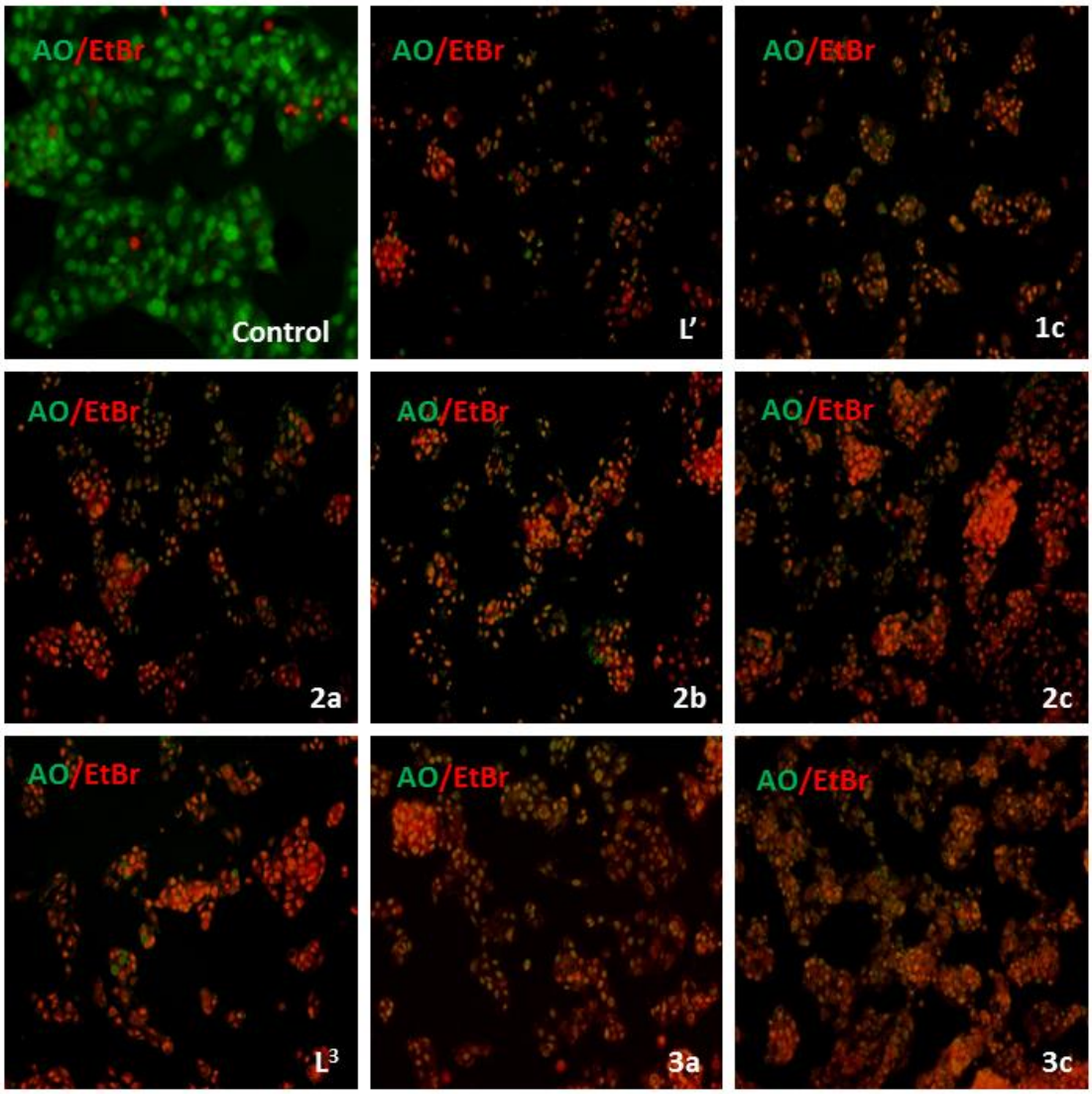

Fig. 7: Acridine Orange (AO)-Ethidium Bromide (EB) staining for detection of live and Apoptotic cells-Green denotes live cells with AO stained cells while red dented apoptotic cells stained with EB

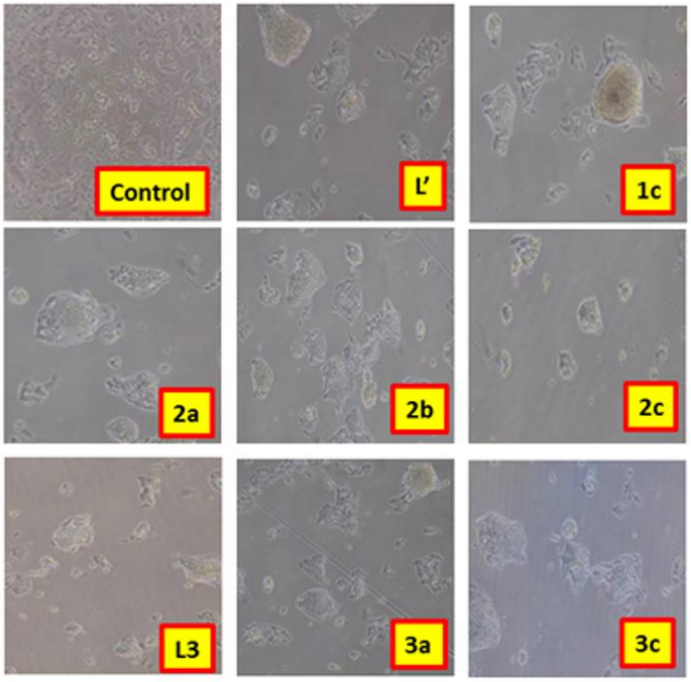

Fig. 8: Phase Contrast images of Hep G2 cells exposed to the potential compounds **L', 1c, 2a, 2b, 2c, L^3**, **3a, 3b** and **3c** compared to the control indicating the *in-vitro* cytotoxic activity. These compounds were assayed at their respective *in-vitro* growth inhibitory IC_{50} value, as determined using the MTT assay in Hep G2 cells.

The morphological investigation carried out by using microscopic photographs of Hep G2 upon 24 h exposure to the potent compounds and standard cisplatin at their respective *in vitro* IC_{50} values (Fig. 8) undoubtedly differentiate the normal proliferation of cells without any insult (control) from less proliferation of cells upon exposure to all the synthesized compounds. The enhanced bio-activity of these macrocyclic compounds is apparently associated with possible hydrogen bonding interaction with bio-molecules due to outward projections of amide groups while the ease of accessibility through the cell membrane is attributed to the presence of hydrophobic cavity created by inward inclination of sulfurs (vide supra). However, further studies are required to explicate the exact mechanism and pathway of apoptosis being followed. The worth of any cytotoxic drug is measured by its property of specificity towards cancer cells over normal healthy cells.[46,47] The exceptional cytotoxicity and specificity of all the compounds for Hep G2 cell line and their ability to induce apoptotic cell death opens the window for further investigation on other cell lines in future.

4.4 Conclusion

This study allows us to conclude that a coordination driven self-assembly of 1,3-bis(2-(alkylamino)acetamido) phenylenes (**L^1-L^3**), CS_2 and Ni^{II}, Cu^{II} or Zn^{II} ions affords access to a novel series of 32-membered neutral binuclear metallomacrocyclic dithiocarbamate complexes of the type [M^{II}_2-μ^2-bis-{(κ^2S,S-$S_2CN(R)CH_2CONH)_2C_6H_4$}] {R = *Cy*, M = Ni^{II} 1a, Cu^{II} 1b, Zn^{II} 1c; R = ^{i}Pr, M = Ni^{II} 2a, Cu^{II} 2b, Zn^{II} 2c; R = ^{n}Bu, M = Ni^{II} 3a, Cu^{II} 3b, Zn^{II} 3c}. Interestingly, X-ray structure of L' demonstrates the formation of an unusual C-Cl…π intermolecular contacts along with C-H…Cl, CH...O and N-H...O interactions leading to a fascinating 2D infinite supramolecular sheet. As expected, cytotoxic activity of a majority of compounds ca **L', L^1, 1a, 1b, 1c, 2a, 2b, 2c, L^3, 3a, 3b, 3c** is found multi-fold better than Cisplatin and specificity for carcinoma Hep G2 over normal liver cell line (WRL-68). For instance, compound **2c** (IC50: 4.80 ± 0.42 µM) exhibit almost 15 fold, **1c (**IC50: 13.78 ± 0.50 µM**)** and **2a (**IC50: 11.40 ± 0.32 µM**)** 5-6 fold; **1a** (IC50: 20.14 ± 0.50µM), **1b** (IC50: 36.35 ± 0.52µM), **2b** (IC50: 20.07 ± 0.37µM) and **3b** (IC50: 20.90 ± 0.40µM) 3-2 fold improved cytotoxic activity than the reference drug cispaltin (IC50: 75.67 ± 0.33 µM). The shrinking of cells can be clearly visualized by acridine orange/ethidium bromide (AO/EB) staining indicating the induction of apoptosis as part of the mechanism of action of these compounds. MESP clearly reveals a number of donor-acceptor sites explaining effective interactions of metallomacrocyclic compounds with biomolecules.

4.5 References

[1] (a) R. Kieltyka, P. Englebienne, J. Fakhoury, C. Autexier, N. Moitessier, H. F. Sleiman, *J. Am. Chem. Soc*. **2008**, *130*, 10040. (b) E.M. Driggers, S. P. Hale, J.Lee, N. K. Terrett, *Nat. Rev. Drug Discov*. **2008**, *7*, 608. (c) J. Mallinson, I.Collins, *Future Med. Chem*., **2012**, *4*, 1409.

[2] (a) K. N. Burger, R. W. Staffhorst, H. C. de Vijlder, M. J. Velinova, P. H. Bomans, P. M. Frederik, B. de Kruijff, *Nat. Med.* **2002**, *8*, 81. (b) Z. Yang, X. Wang, H. Diao, J. Zhang, H. Li, H. Sungand, Z. Guo, *Chem. Commun*. **2007**, 3453. (c) N. J. Wheate, A. I. Day, R. J. Blanch, A. P.Arnold, C. Cullinane, J. G. Collins, *Chem. Commun*. **2004**, 1424. (d) C. Sanchez-Cano, M. J Hannon, *Dalton Trans.* **2009**, 10702. (e) A. M. Krause-Heuer, N. J. Wheate, M. J. Tilby, D. G. Pearson, C. J. Ottley, J. R. Aldrich-Wright, *Inorg. Chem*. **2008**, *47*, 6880.

[3] (a) J. Olguín, M. Kalisz, R. Clérac, S. Brooker, *Inorg. Chem*. **2012**, *51*, 5058. (b) A. L. Gavrilova, B. Bosnich, *Chem. Rev*. **2004**, *104*, 349. (c) J. Klingele, S. Dechert, F. Meyer, *Coord. Chem. Rev*. **2009**, *253*, 2698. (d) T. W. Hambley, *Dalton Trans*. **2007**, 4929. (e) C. Orvig, M. J. Abrams, *Chem. Rev*. **1999**, *99*, 2201. (f) K. H. Thompson, C. Orvig, *Dalton Trans*. **2006**, 761.

[4] (a) Y. W. Jung, S. J. Lippard, *Chem. Rev*. **2007**, *107*, 1387. (b) S. K. Singh, S. Joshi, A. R. Singh, J. K. Saxena, D. S. Pandey, *Inorg. Chem*. **2007**, *46*, 10869. (c) R. K. Gupta, R. Pandey, G. Sharma, R. Prasad, B. Koch, S. Srikrishna, P.-Z. Li, Q. Xu, D. S. Pandey, *Inorg. Chem*. **2013**, *52*, 3687. (d) R. K. Gupta, G. Sharma, R. Pandey, A. Kumar, B. Koch, P.-Z. Li, Q. Xu, D. S. Pandey, *Inorg. Chem*. **2013**, *52*, 13984.

[5] A. Alama, B. Tasso, F. Novelli, F. Sparatore, *Drug Discovery Today*, **2009**, *14*, 500.

[6] (a) Y. Suda, A. Arano, Y. Fukui, S. Koshida, M. Wakao, T. Nishimura, S. Kusumoto, M. Sobel, *Bioconjugate Chem*. **2006**, *17*, 1125. (b) A. B. Mahon, P. S. Arora, *Chem*. *Commun*. **2012**, *48*, 1416. (c) S. A. Stoffregen, A. K. K. Griffin, N. M. Kostic, *Inorg*. *Chem*. **2005**, *44*, 8899. (d) S. J. Dougan, A. Habtemariam, S. E. McHale, S. Parsons, P. J. Sadler, *Proc. Natl. Aacad. Sci. U.S.A.*, **2008**, *105*, 11628. (e) B. P. Espósito, R. Najjar, *Coord. Chem. Rev*. **2002**, *232*, 137.

[7] (a) M. Bousseau, L. Valade, J.P. Legros, P. Cassoux, M. Garbaukas, L.V. Interrante, *J. Am. Chem. Soc.* **1989**, *108*, 1908. (b) A. T. Coomber, D. Beljonne, R. H. Friend, J. L. Bredas, A. Charlton, N. Robertson, A. E. Underhill, M. Kurmoo, P. Day, *Nature*, **1996**, *380*, 144. (c) N. Singh, V. K. Singh, *Trans. Met. Chem*. **2001**, *26*, 435. (d) Nanhai Singh, Vinay K. Singh, *Synth. Reac. Inorg. Met.-Org. Chem*. **2001**, *31*, 1743. (e) Nanhai Singh, Vinay K. Singh, *Trans. Met. Chem.* **2002**, *27*, 359. (f) J.D.E.T. Wilton-Ely, D. Solanki, E.R. Knight, K.B. Holt, A.L. Thompson, G. Hogarth, *Inorg. Chem*. **2008**, *47*, 9642.

[8] (a) S. Banerjee, G.R. Kumar, P. Mathur, P. Sekar, *Chem. Commun*. **1997**, 299. (b) P. Mathur, D.K. Rai, R. ShyamJi, B. Pathak, S. Boodida, S.M. Mobin, *RSC Adv.*, **2013**, *3*, 26025. (c) P. Mathur, S. Mukhopadhyay, M.O. Ahmed, G.K. Lahiri, S. Chakraborty, M. G. Walawalkar, *Organometallics* **2000**, *19*, 5787. (d) R.K. Gupta, R. Pandey, R. Singh, N. Srivastava, B. Maiti, S. Saha, P. Li, Q. Xu , D.S. Pandey, *Inorg. Chem.* **2012**, *51*, 8916.

[9] Edmundo Guzmán-Percástegui, Lev N. Zakharov,José G. Alvarado-Rodríguez, Matthew E. Carnes, Darren W. Johnson, *Cryst. Growth Des.* **2014**, 14, 2087 *and references cited in.*

[10] (a) R. Kadu, H. Roy, V. K. Singh, *Appl. Organomet. Chem.* **2015**, *29*, 746. (b) V. K. Singh, R. Kadu, H. Roy, P. Raghavaiah, S. M. Mobin, *Dalton Trans.* **2016**, *45*, 1443.

[11] (a) J. M. Humphrey, A. R. Chamberlin, *Chem. Rev*. **1997**, *97*, 2243. (b) Schotten, C. Ber. Dtsch. *Chem. Ges*. **1884**, *17*, 2544. (c) T. Sano, T. Sugaya, K. Inoue, S.-O. Mizutaki, Y. Ono, M. Kasai, *Org. Process Res. Dev*. **2000**, *4*, 147.

[12] (a) S. Faulkner, S. J. A. Pope, B. P. Burton-Pye, *Appl.Spectrosc. Rev*. **2004**, *40*, 1 (b) J. R. Morrow, S. Amin, C. H. Lake, M. R. Churchill, *Angew. Chem., Int. Ed. Engl*. **1994**, *33*, 773. (c) U. Baykal, E. U. Akkaya, *Tetrahedron Lett*. **1998**, *39*, 5861. (d) L. L. Chappell, D. A., Jr. Voss, W. DeW. Jr. Horrocks, J. R. Morrow, *Inorg. Chem*. **1998**, *37*, 3989.

[13] (a) T. Gunnlaugsson, J. P. Leonard, *Chem. Commun*. **2005**, 3114. (b) J. P. Leonard, T. Gunnlaugsson, J. Fluoresc. **2005**, *15*, 585. (c) T. Gunnlaugsson, J. E. O'Brien, S. Mulready, *Tetrahedron Lett*. **2002**, *43*, 8493. (d) T. Gunnlaugsson, D. A. MacDo´ nail, D. J. Parker, *Am.Chem. Soc*. **2001**, *123*, 12866. (e) T. Gunnlaugsson, A. J. Harte, *Org. Biomol. Chem*. **2006**, *4*, 1572.

[14] (a) T. Gunnlaugsson, A. J. Harte, J. P. Leonard, M. Nieuwenhuyzen, *Chem. Commun*. **2002**, 2134. (b) T. Gunnlaugsson, J. P. Leonard, *Dalton Trans*. **2005**, 3204. (c) T. Gunnlaugsson, J. P. Leonard, *Chem. Commun*. **2003**, 2424. (d) T. Gunnlaugsson, *TetrahedronLett.* **2001**, *42*, 8901. (e) T. Gunnlaugsson, J. P. Leonard, K. Sénéchal and A. J. Harte, *Chem. Commun*. **2004**, 782. (f) T. Gunnlaugsson, R. J. H. Davies, M. Nieuwehuyzen, C. S. Stevenson R. Viguier, S. Mulready, *Chem.Commun*. **2002**, 2136.

[15] E. K. Farrell, D. J. Merkler, *Drug Discov Today*, **2008**, *13*, 558–568.

[16] Y. Chung, Y. A, Do-Heyoung Kim, Y. Kwon, *Journal of Power Sources*, **2017**, 337, 152.

[17] S. Yamaki, D. Suzuki, J. Fujiyasu, M. Neya, A. Nagashima, M. Kondo, T. Akabane, K. Kadono, A. Moritomo, K. Yoshihara, *Bioorg. Med. Chem.* **2017**, *25*, 187–201.

[18] H. S. Samaha, R. Hamid, K. El-Bayoumy, C.V. Rao, B. S. Reddy, *Cancer Epidemiol. Biomarkers Prev*., **1997**, *6*, 699.

[19] D. G. Colak, I. Cianga, D. O. Demirkol, O. Kozgus, E. I. Medine, S. Sakarya, P. Unak, S. Timur, Y. Yagci, *J. Mater. Chem*. **2012**, *22*, 9293.

[20] M. Yuksel, D. G. Colak, M. Akin, I. Cianga, M. Kukut, E. I. Medine, M. Can, S. Sakarya, P. Unak, S. Timur, Y. Yagci, *Biomacromolecules*, **2012**, *13*, 2680.

[21] D. Ag, M. Seleci, R. Bongartz, M. Can, S. Yurteri, I. Cianga, F. Stahl, S. Timur, T. Scheper, Y. Yagci, *Biomacromolecules*, **2013**, *14*, 3532.

[22] W. Wang, R. Li, G. W. Gokel, *Chem. Eur. J*. **2009**, *15*, 10543.

[23] (a) P. D. Beer, N. G. Berry, A. R. Cowley, E. J. Hayes, E. C. Oates, W. W. H. Wong, Chem. Commun. **2003**, 2408–2409. (b) P. D. Beer, Neil Berry, Michael G. B. Drew, O. Danny Fox, M. E. Padilla-Tosta, S. Patell, *Chem. Commun.* **2001**, 199.

[24] S. K. Verma, V. K. Singh, *RSC Adv*. **2015**, *5*, 53036. (b) S. K. Verma, V. K. Singh, *J. Organomet. Chem*. **2015**, *791*, 214.

[25] V. Pillai, R. Kadu, L. Buch, V. K. Singh, *ChemistrySelect*, **2017**, *2*, 4382.

[26] S. Leininger, B. Olenyuk, P. J. Stang, *Chem. Rev*. **2000**, *100*, 853.

[27] C. J. Jones, *Chem. Soc. Rev*. **1998**, *27*, 289.

[28] G. Ercolani, *J. Phys. Chem. B*. **2003**, *107*, 5052.

[29] (a) V. K. Singh, R. Kadu, H. Roy, *Eur. J. Med. Chem*. **2014**, *74*, 552.

[30] R. Kadu, V. Pillai, V. Amrit, V. K. Singh, *RSC Adv*. **2015**, *5*, 106688.

[31] B. F. Ali, W. S. Al- Akramawi, K. H. Al- Obaidi, A. H. A. Al-Karboli, *Thermochimica Acta*, **2004**, *419*, 39.

[32] (a) P. D. Beer, A. G. Cheetham, M. G. B. Drew, O. Danny Fox, J. Elizabeth Hayes, T. D. Rolls, *Dalton Trans*. **2003**, *4*, 603. (b) J. Cookson, E. A. L. Evans, J. P. Maher, C. J. Serpell, R. L. Paul, A. R. Cowley, M. G. B. Drew, P. D. Beer, *Inorg. Chim. Acta*, **2010**, *363*, 1195. (c) Siu-Wai Lai, M. G. B. Drew, P. D. Beer, *J. Organomet. Chem*. **2001**, *637–639*, 89.

[33] R. Kadu, V. K. Singh, S. K Verma, P. Raghavaiah, M. M. Shaikh, *J. Mol. Struct*. **2013**, *1033*, 298.

[34] S. R. Gadre, P. K. Bhadane, *Resonance*, **1999**, *4*, 11. (b) F. A. Bulat, A. T.-Labbé, T. Brinck, J. S. Murray, P. Politzer, *J Mol Model* **2010**, *16*, 1679. (c) P. Politzer, P. R. Laurence, K. Jayasuriya, *Environ. Health Perspect.* **1985**, *61*, 191.

[35] S. K. Verma and V. K. Singh, *RSC Adv*. **2015**, *5*, 43669.

[36] (a) D. Swierczynski, R. Luboradzki, G. Dolgonos, J. Lipkowski, H. –J. Schneider, *Eur. J. Org. Chem*. **2005**, 1172 (b) L. Brammer, G. M. Espallagras, S. Libri, *CrystEngComm*. **2008**, *10*, 1712.

[37] (a) Y. Imai, Y. Inoue, I. Nakanishi, K. Kitaura, *Protein Sci*. **2008**, *17*, 1129; (b) Y. Lu, Y. Wang, W. Zhu, *Phys. Chem. Chem. Phys*. **2010**, *12*, 4543.

[38] F. A. Shah, M. N. Tahir, S. Alia, M. A. Kashmiri, *Acta Cryst.* **2008**, *E64*, 787.

[39] (a) Y. Gu, T. Kar, S. Scheiner, *J. Am. Chem. Soc*. **1999**, *121*, 9411. (b) Z. S. Derewenda, L. Lee, U. Derewenda, *J. Mol. Biol*. **1995**, *252*, 248. (c) G. R. Desiraju, *Acc. Chem. Res*. **1996**, *29*, 441. (d) R. Taylor, O. Kennard, *J. Am. Chem. Soc.* **1982**, *104*, 5063.

[40] (a) G. Mukherjee, K. Biradha, *J. Chem. Sci*. **2014**, *126*, 1285. (b) S. Scheiner, *Phys. Chem. Chem. Phys*. **2011**, *13*, 13860.

[41] (a) M. Nishio, Y. Umezawa, K. Honda, S. Tsuboyama, H. Suezawa, *CrystEngComm*, **2009**, *11*, 1757. (b) S. K. Nayak, R. Sathishkumar, T. N. Guru Row, *CrystEngComm*, **2010**, *12*, 3112. (c) Y. Kobayashi, K. Saigo, *J. Am. Chem. Soc*. **2005**,*127*, 15054. (d) P. Sozzani, A. Comotti, S. Bracco, R. Simonutti, *Chem. Commun*. **2004**, 768.

[42] (a) C. A. Hunter, J. K. M. Sanders, *J. Am. Chem. Soc*. **1990**, *112*, 5525. (c) C. Janiak, *J. Chem. Soc. Dalton Trans*. **2000**, 3885. (c) T. F. Headen, C. A. Howard, N. T. Skipper, M. A. Wilkinson, D. T. Bowron, A. K. Soper, *J. Am. Chem. Soc.* **2010**, *132*, 5735.

[43] M. Sundermann, V. Knasmüller, S. Wu, X. J. Darroudi, F. Kassie, *Toxicology* **2004**, *1–3*, 329.

[44] M. P. Mattson, *Brain Pathology* **2000**, *10*, 300.

[45] K. Liu, P. C. Liu, R. Liu, X.Wu, *Medical science monitor basic research* **2015**, *21*, 15.

[46] (a) S. Kemp, N. J. Wheate, M. P. Pisani, J. R. Aldrich-Wright, *J. Med. Chem*. **2008**, *51*, 2787. (b) N. J. Wheate, *J. Inorg. Biochem*. **2008**, *102*, 2060.

[47] A. K. Taraphdar, M. Roy, R.Bhattacharya, *Curr Sci.* **2001**, *80*, 1387.

[48] Oxford Diffraction, CrysAlis PRO, Oxford Diffraction Ltd., Yarnton, England, **2009**.

[49] O. V. Dolomanov, L. J. Bourhis, R. J. Gildea, J. A. K. Howard, H. Puschmann *J. Appl. Cryst.* **2009**, *42*, 339-341.

[50] G. M. Sheldrick, *ActaCrystallogr C Struct Chem*. **2015**, *71*, 3–8.

4.6 Annexures:

4.6.1. Spectral Characterization

Mass Spectra:

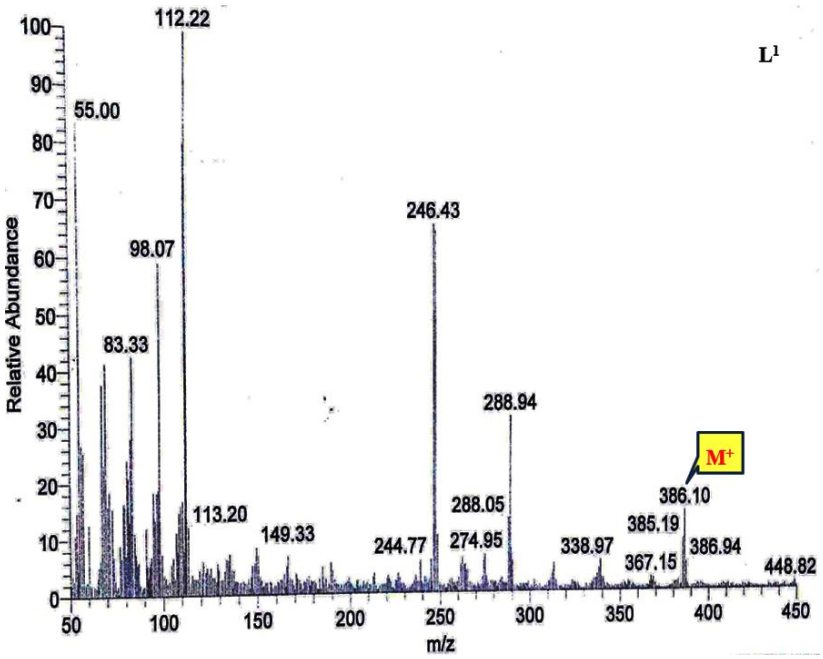

Annexure 1. Mass spectrum of $\mathbf{L^1}$

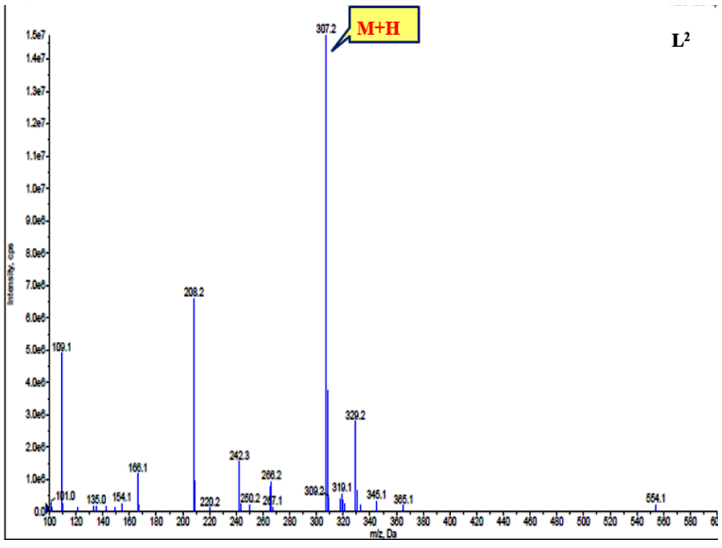

Annexure 2. Mass spectrum of $\mathbf{L^2}$

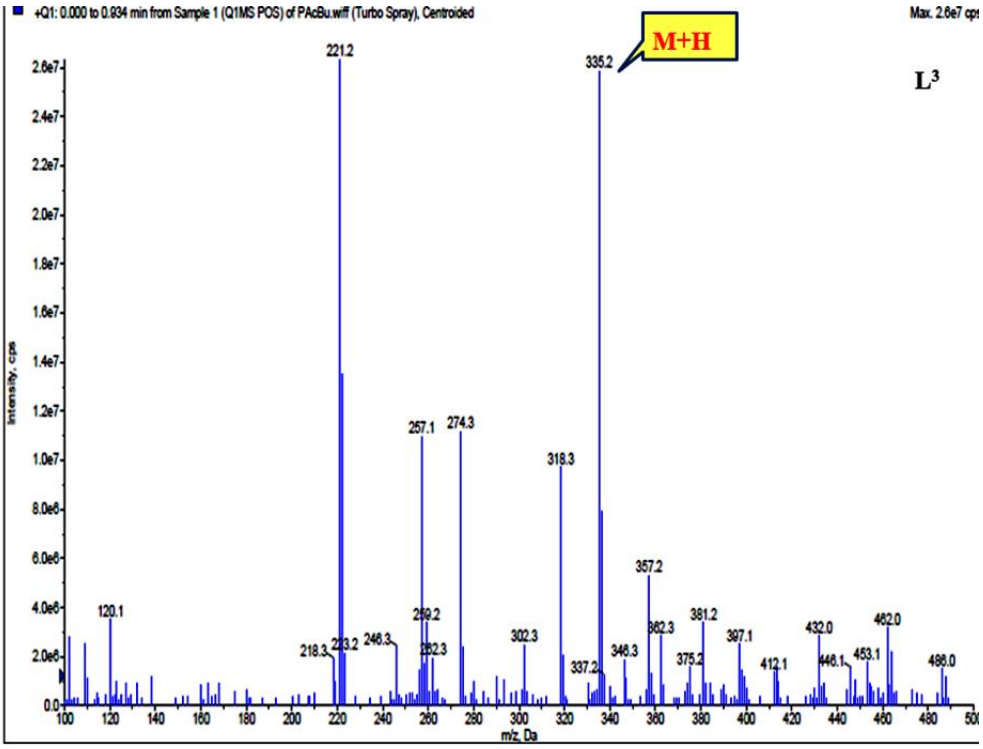

Annexure 3. Mass spectrum of $\mathbf{L^3}$

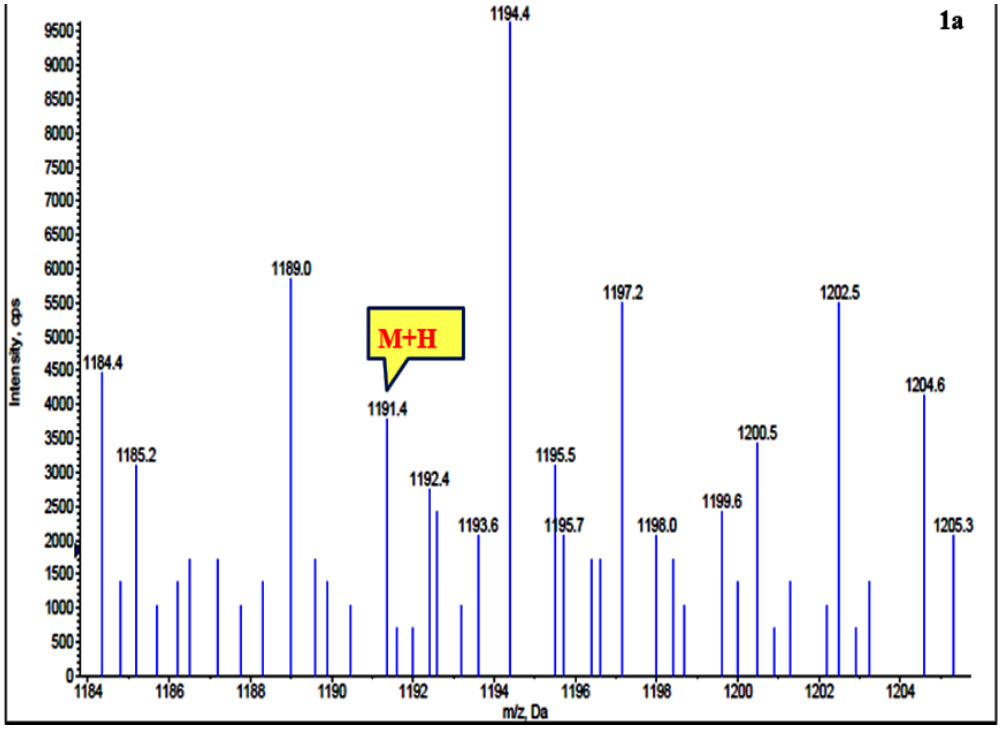

Annexure 4. Mass spectrum of **1a**

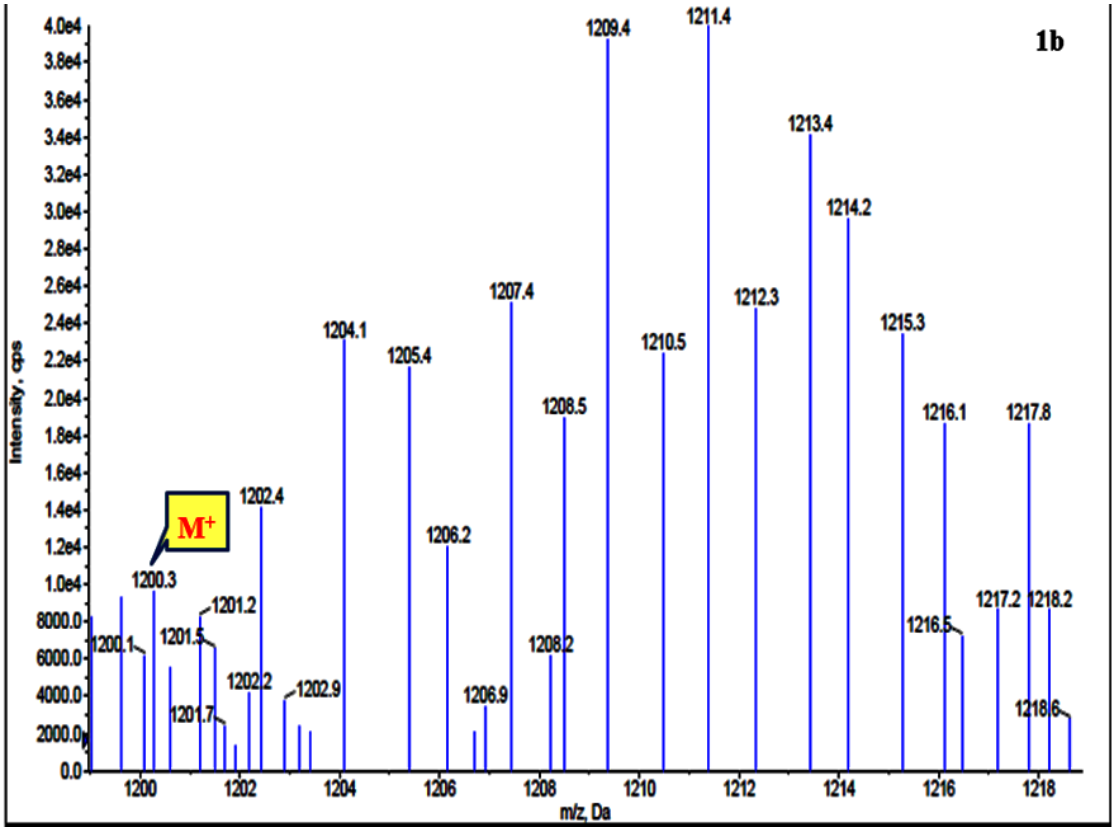

Annexure 5. Mass spectrum of **1b**

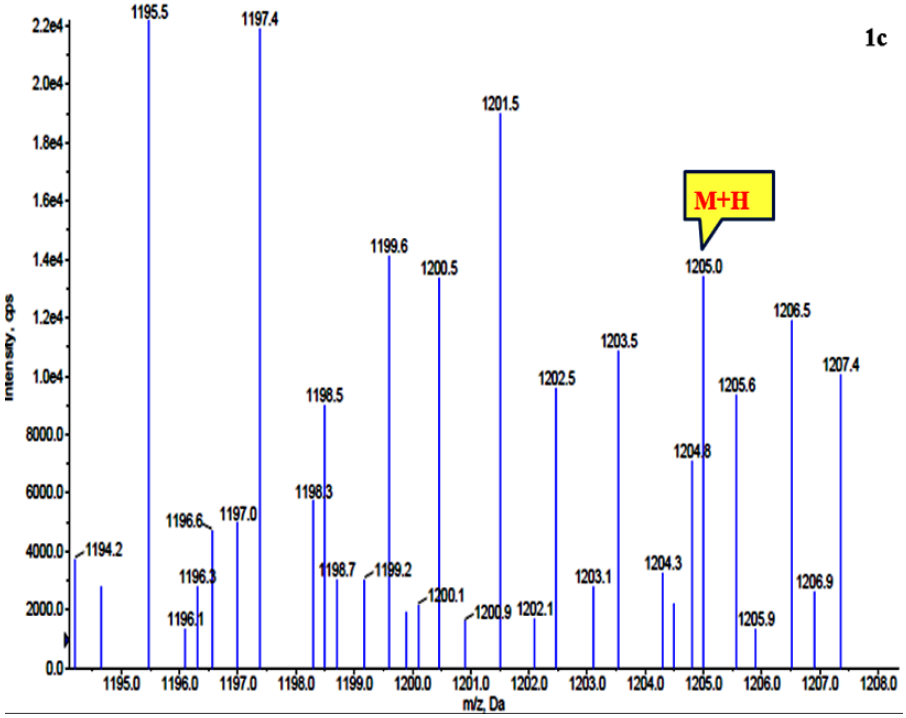

Annexure 6. Mass spectrum of **1c**

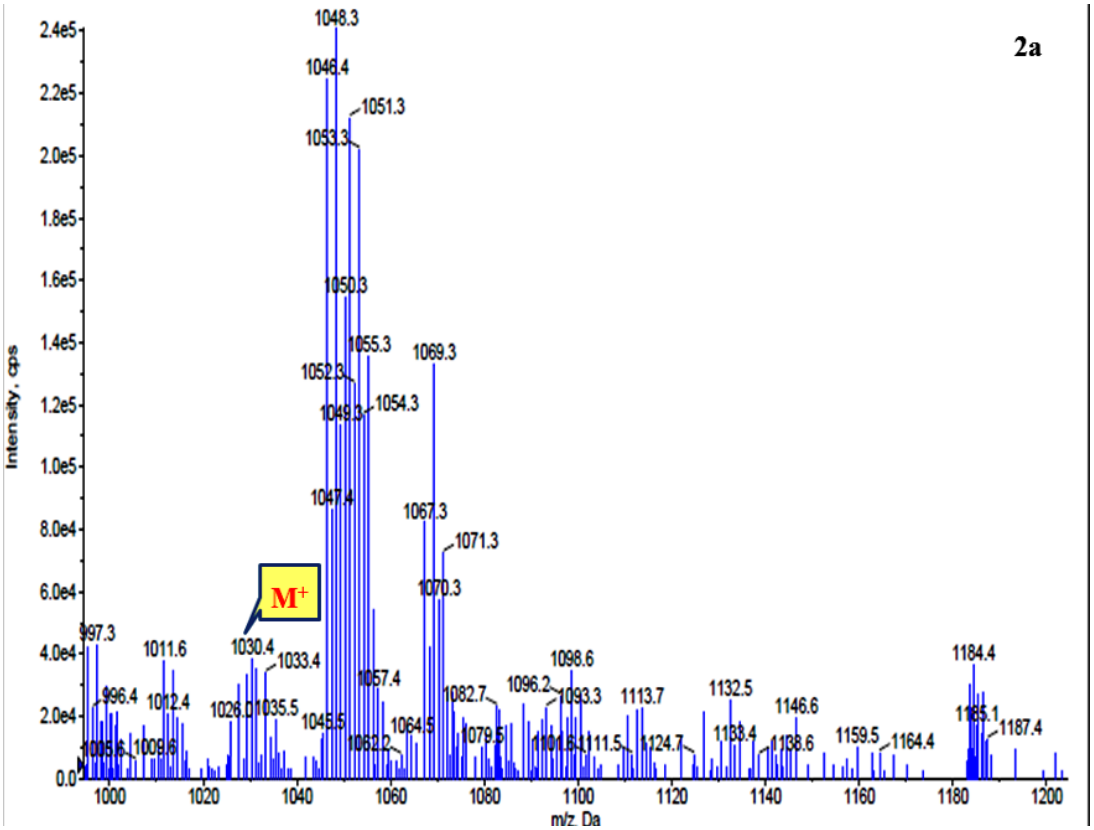

Annexure 7. Mass spectrum of **2a**

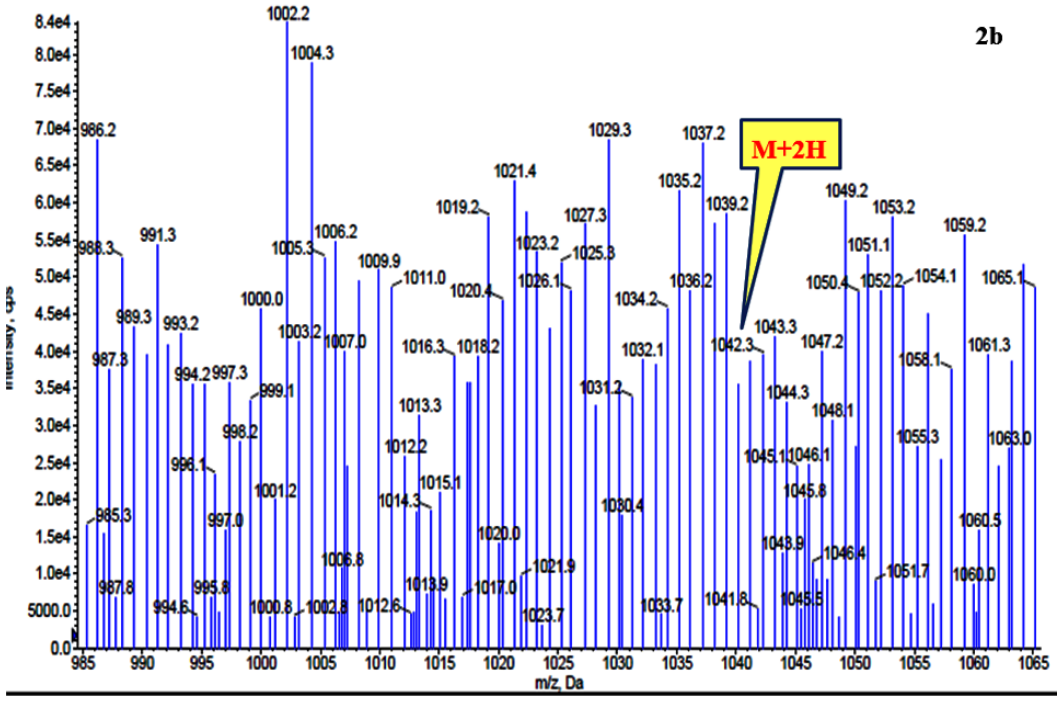

Annexure 8. Mass spectrum of **2b**

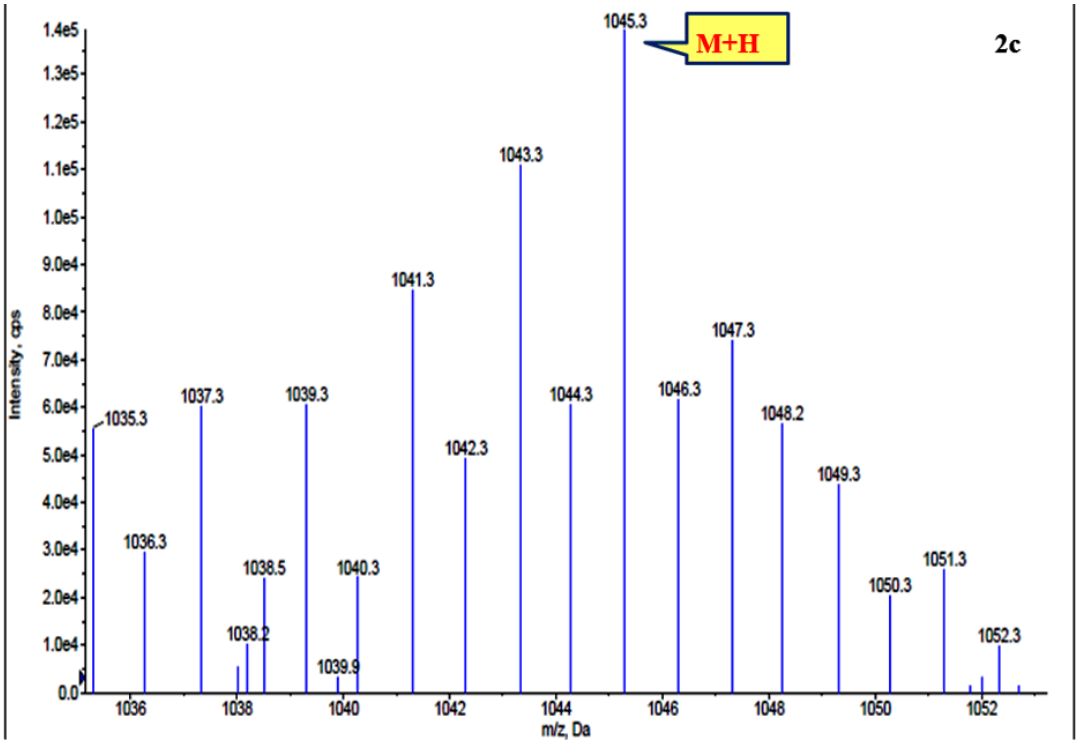

Annexure 9. Mass spectrum of **2c**

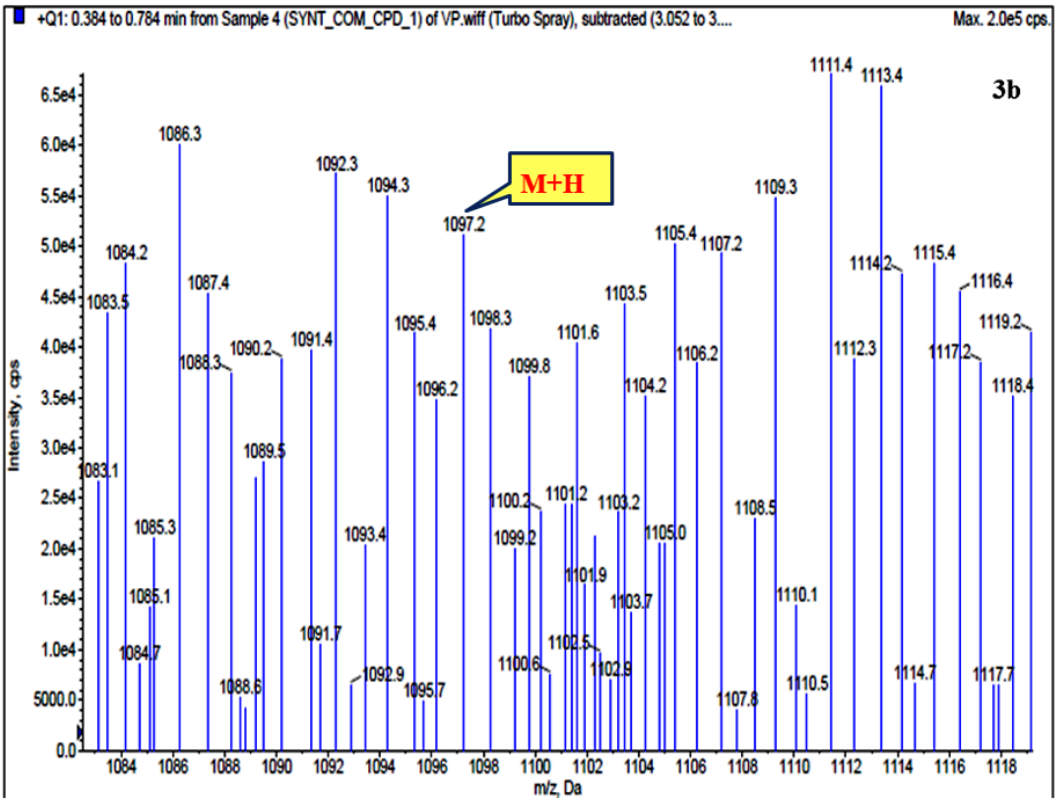

Annexure 10. Mass spectrum of **3b**

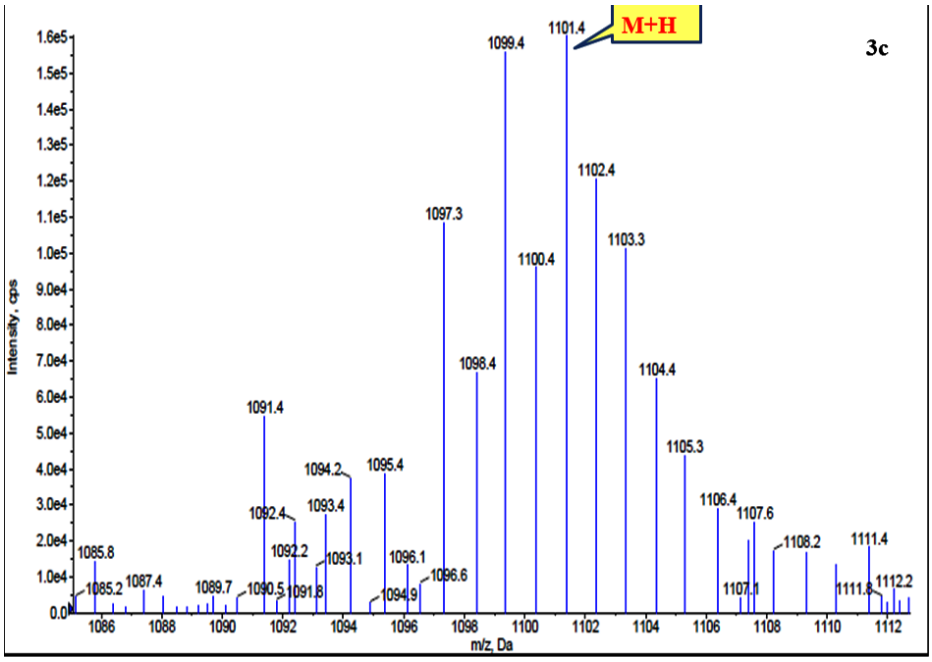

Annexure 11. Mass spectrum of **3c**

IR spectral data:

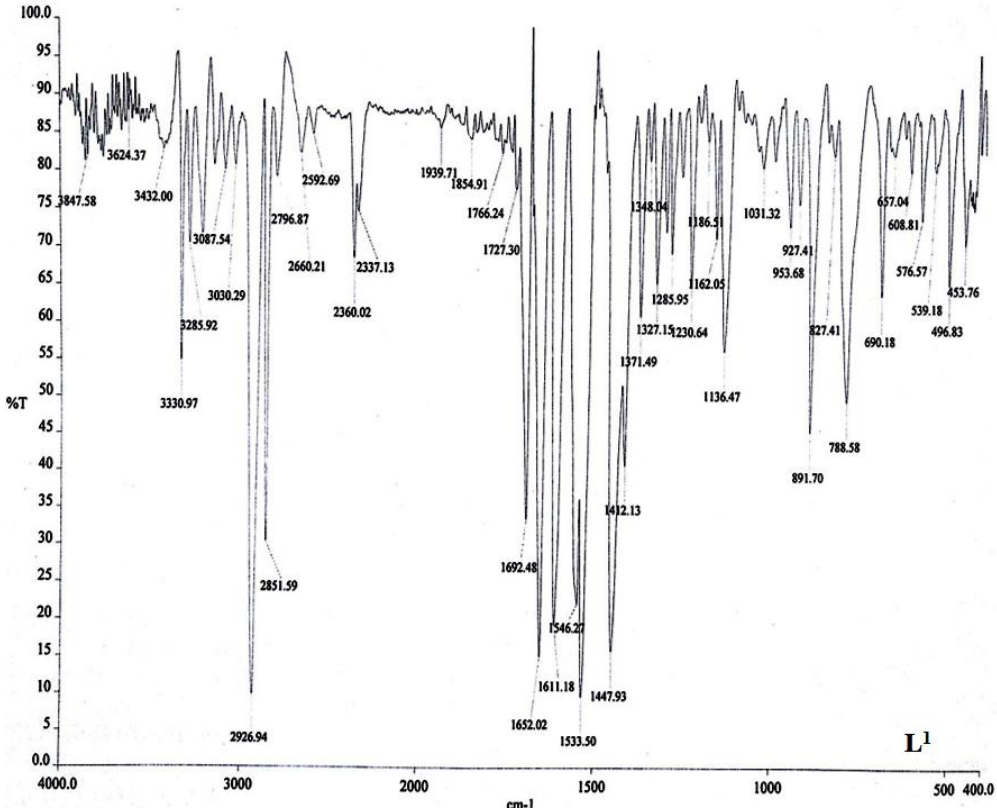

Annexure 12. IR spectrum of L^1

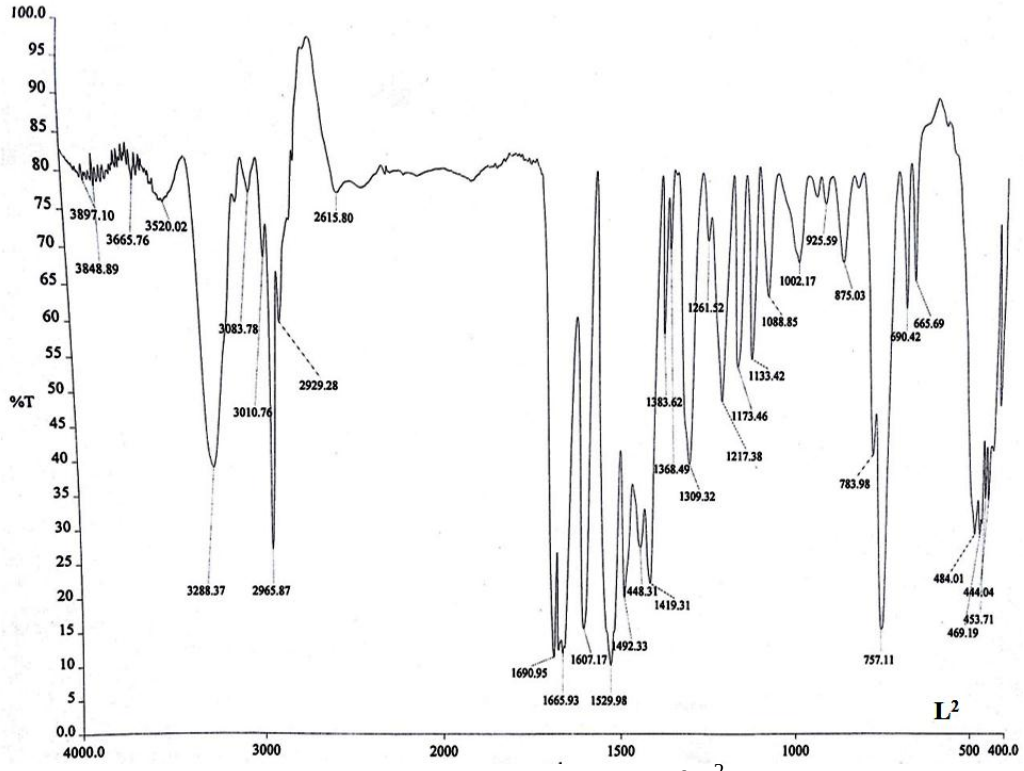

Annexure 13. IR spectrum of L^2

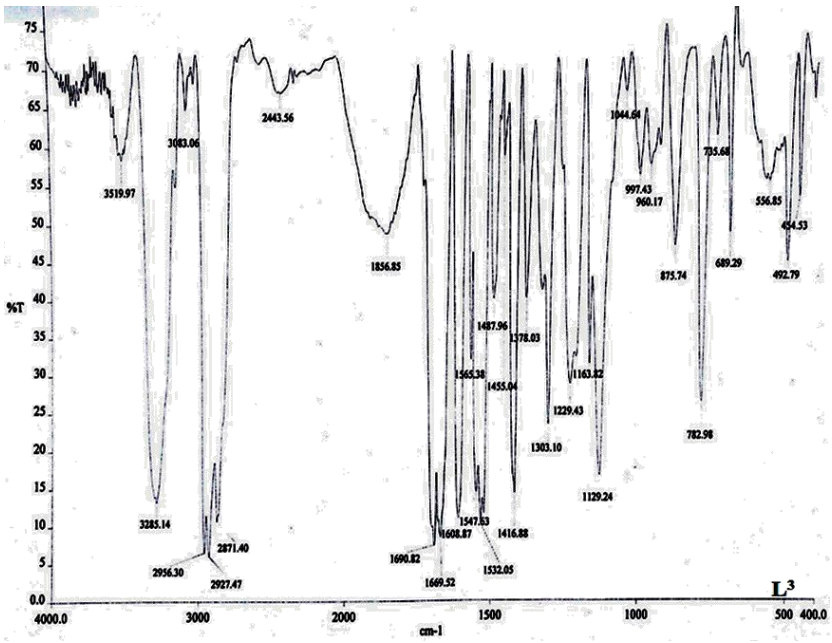

Annexure 14. IR spectrum of L^3

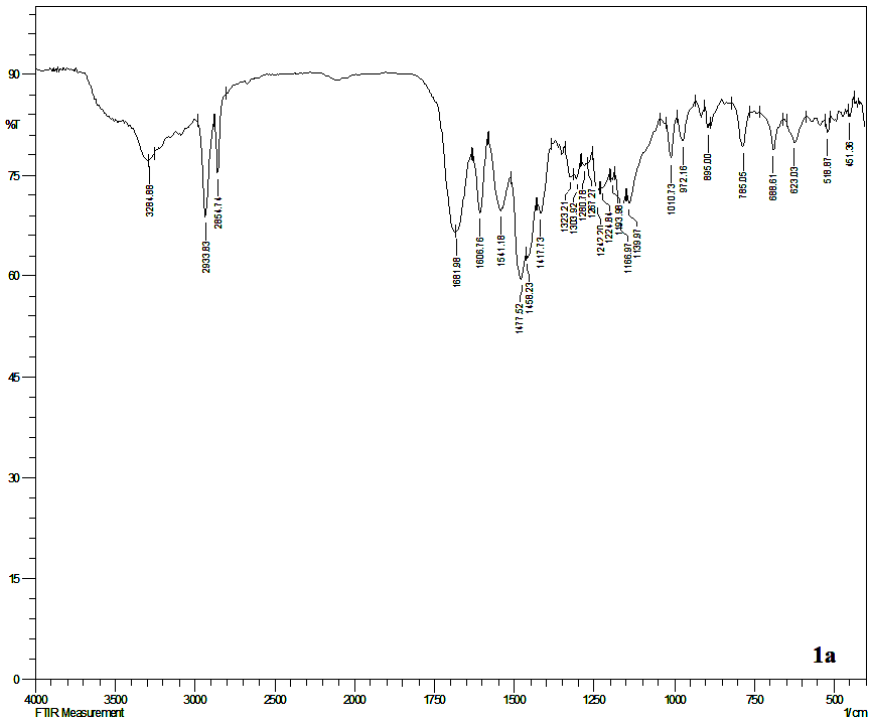

Annexure 15. IR spectrum of 1a

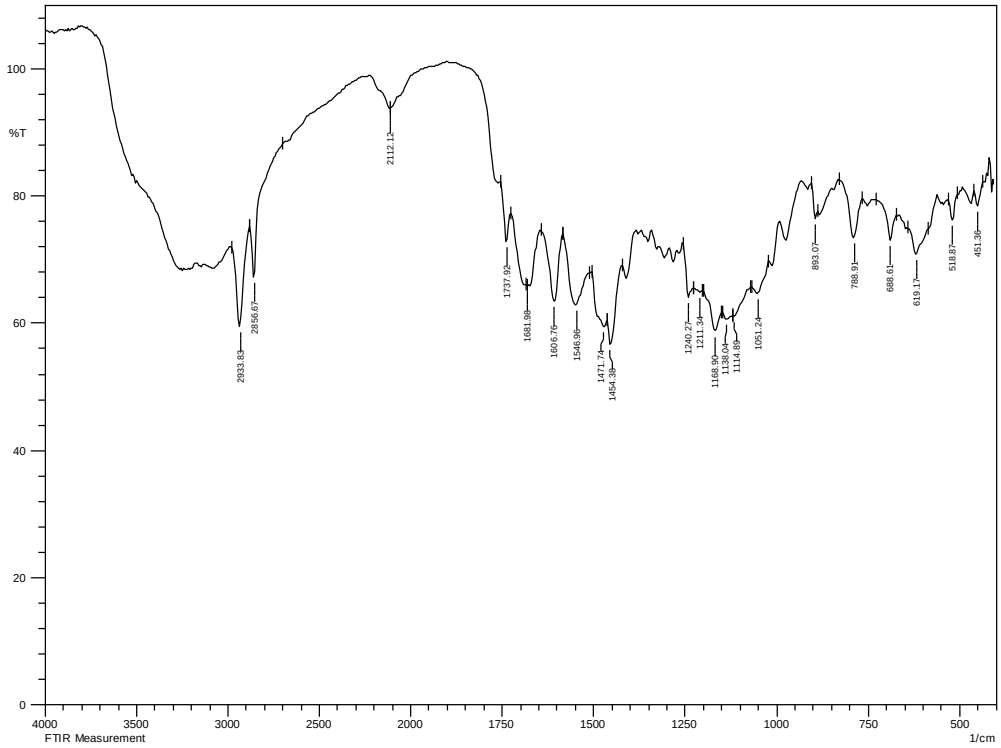

Annexure 16. IR spectrum of 1b

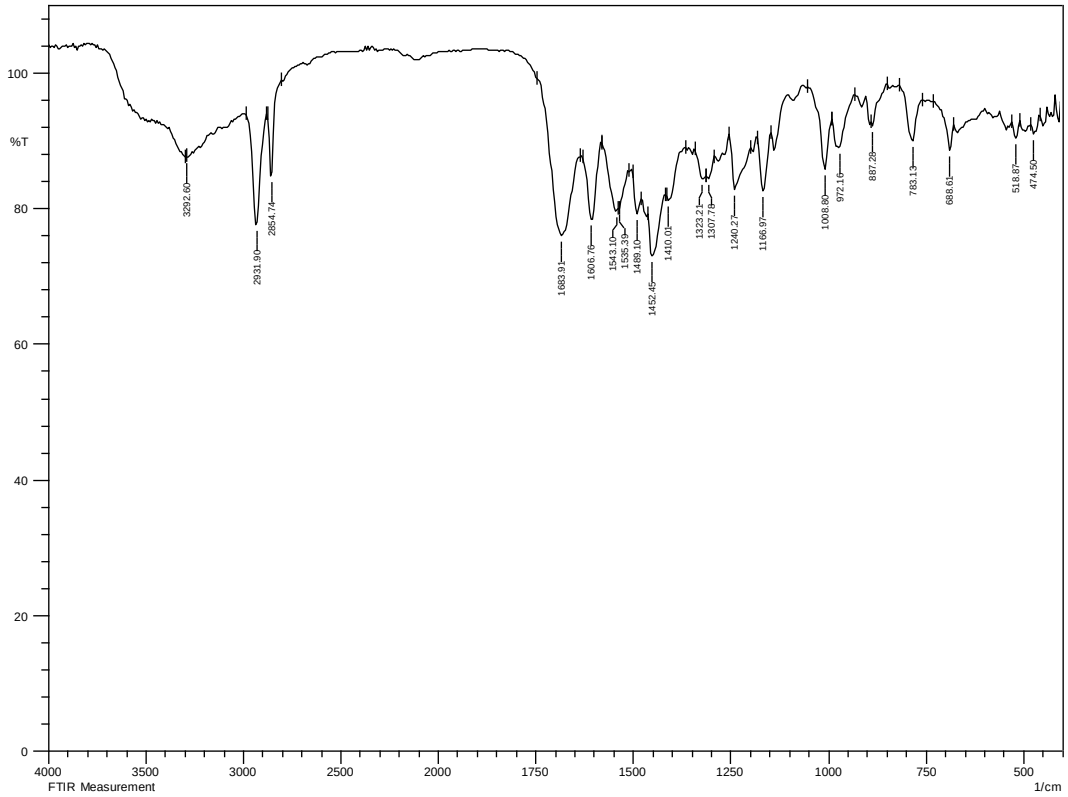

Annexure 17. IR spectrum of 1c

NMR spectral data:

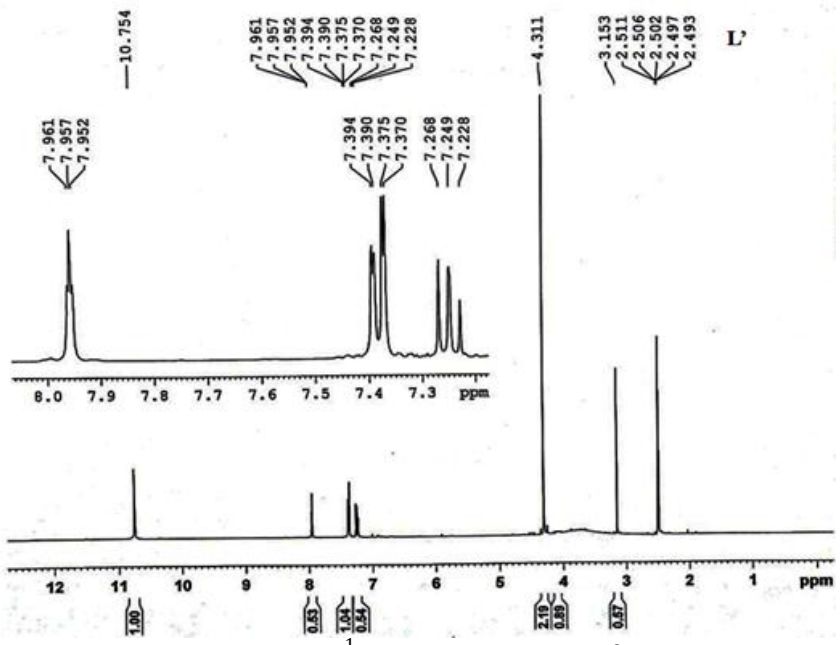

Annexure 18. ^{1}H NMR spectrum of **(L')**

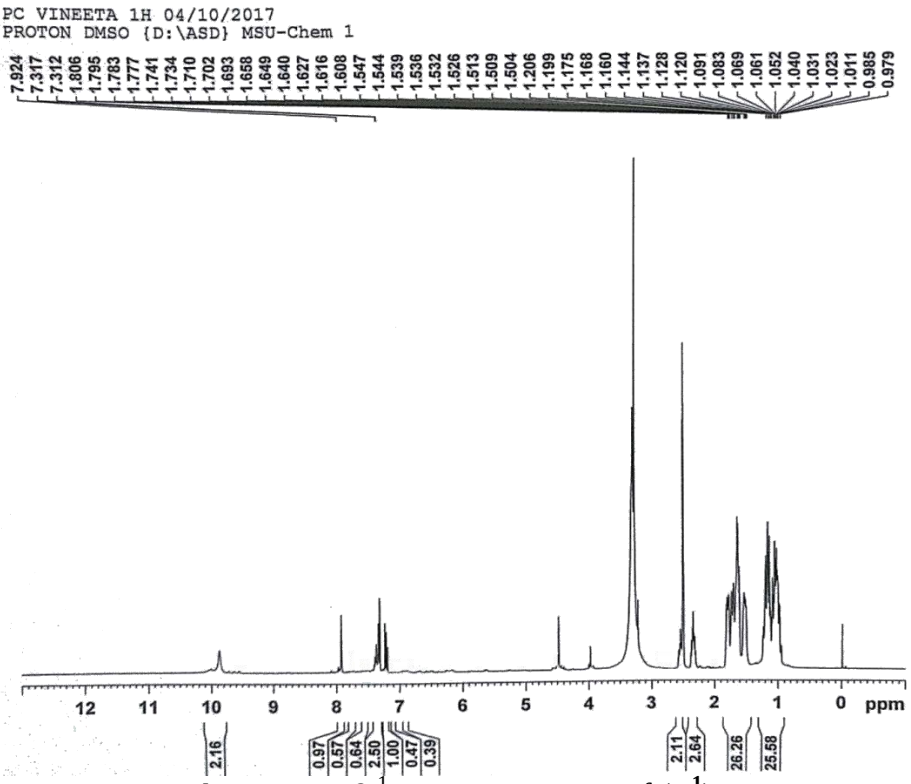

Annexure 19. ^{1}H NMR spectrum of **(L^1)**

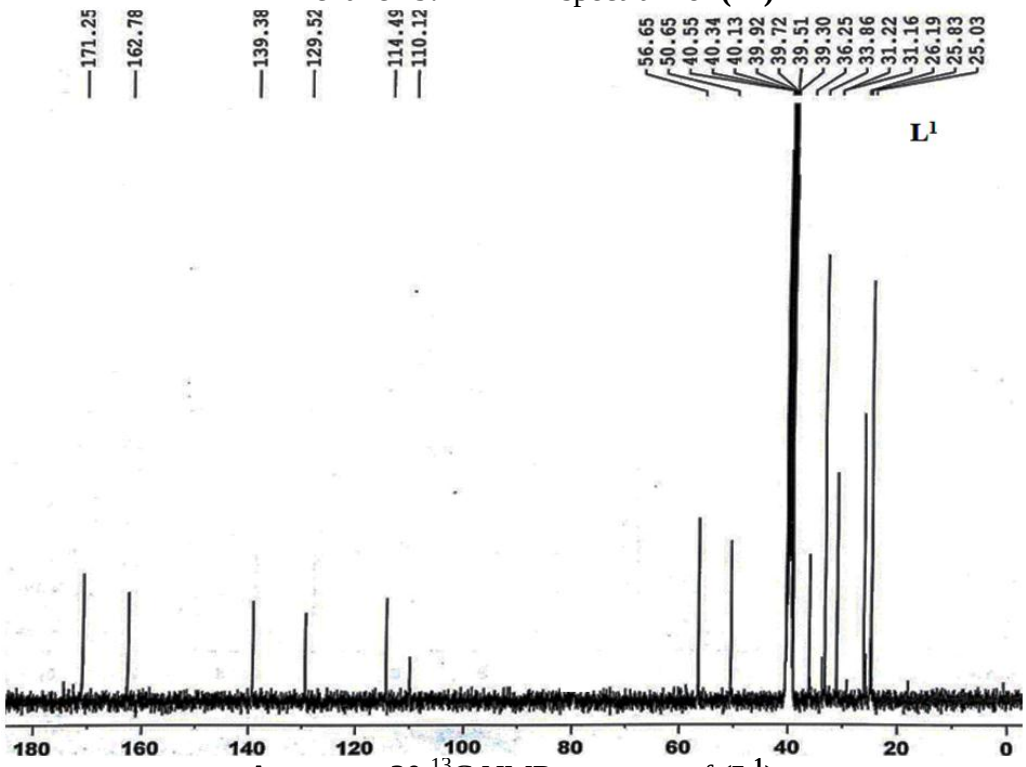

Annexure 20. ^{13}C NMR spectrum of **(L^1)**.

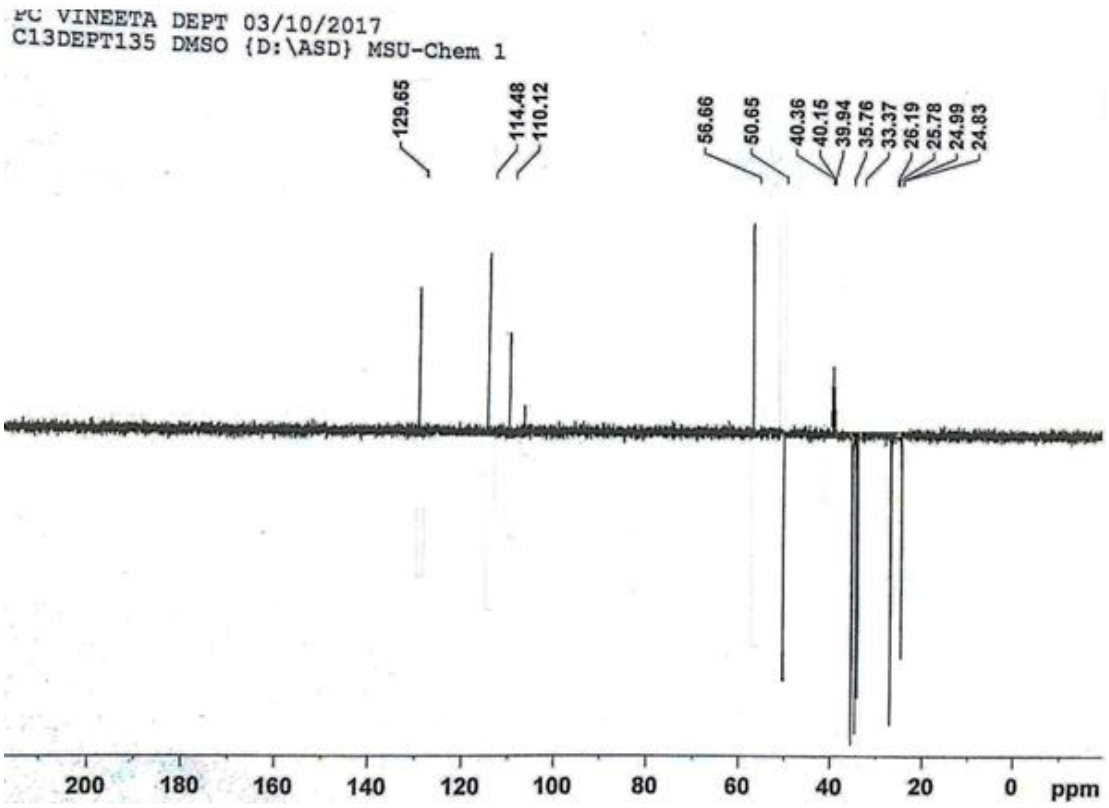

Annexure 21. DEPT 135 NMR spectrum of **(L^1).**

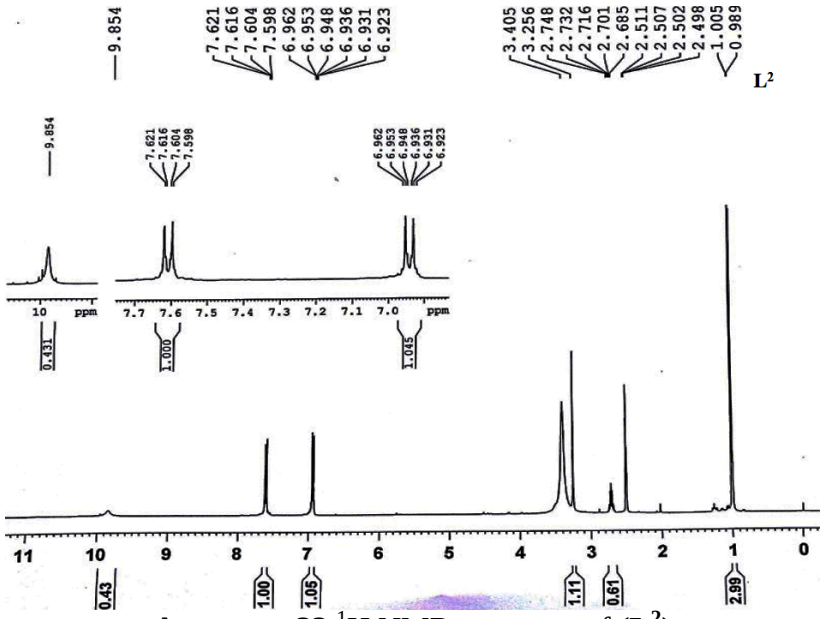

Annexure 22.^{1}H NMR spectrum of **(L^2)**

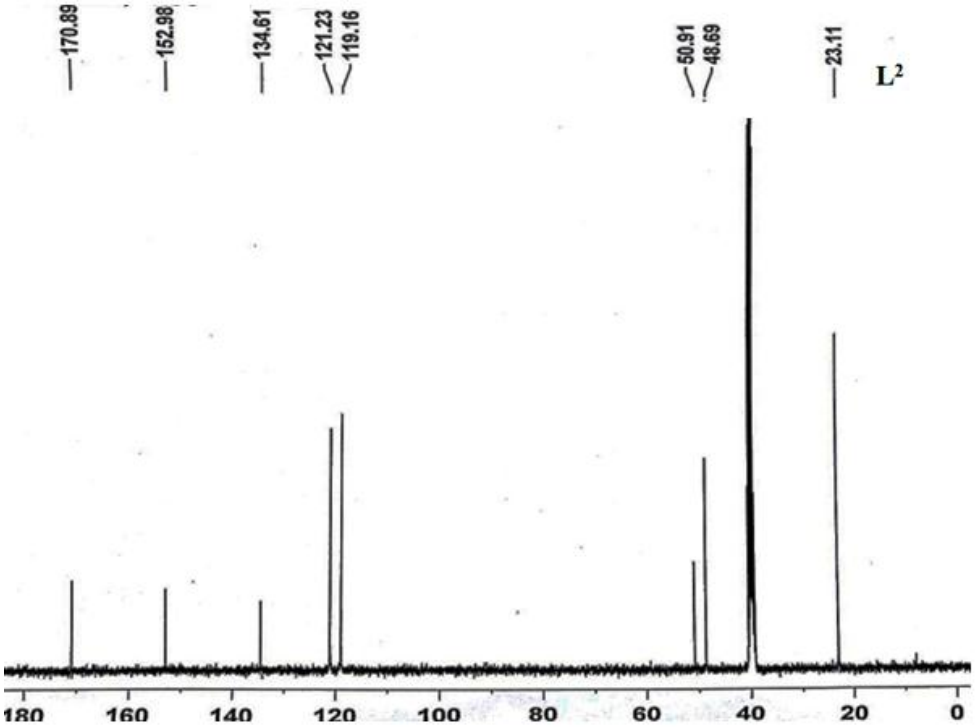

Annexure 23. ^{13}C NMR spectrum of **(L^2)**

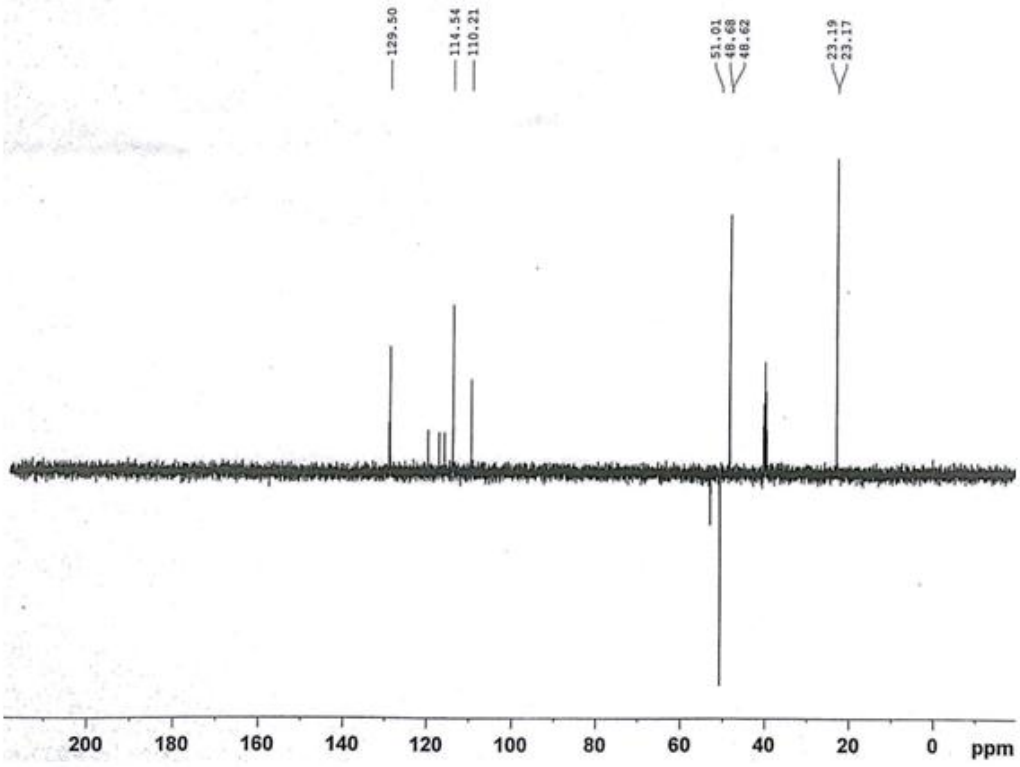

Annexure 24. DEPT 135 NMR spectrum of **(L^2)**

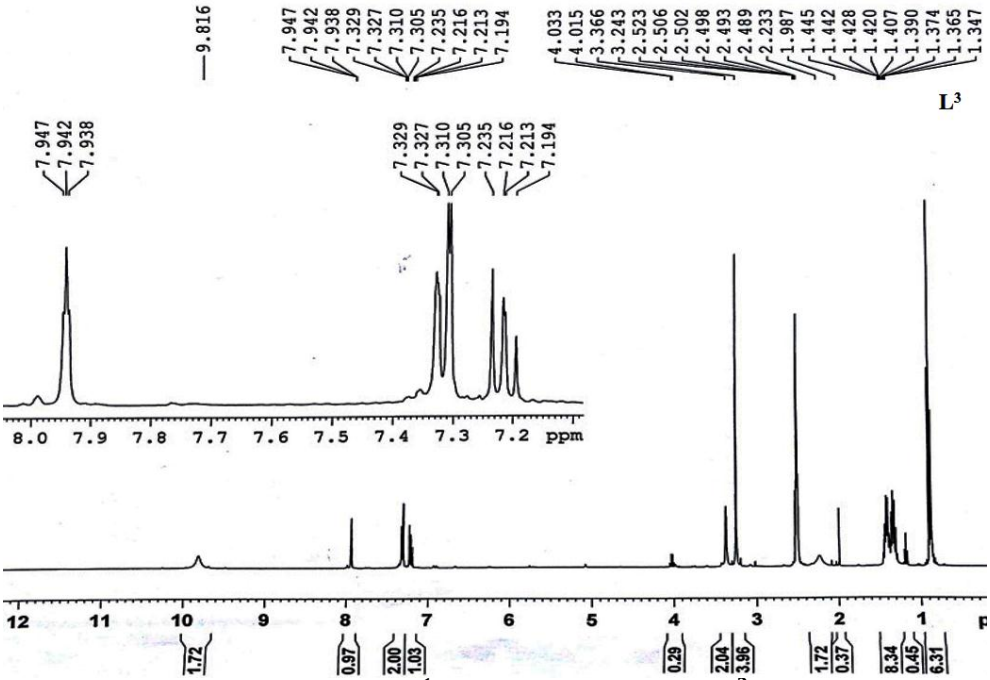

Annexure 25. ^{1}H NMR spectrum of **(L^3)**

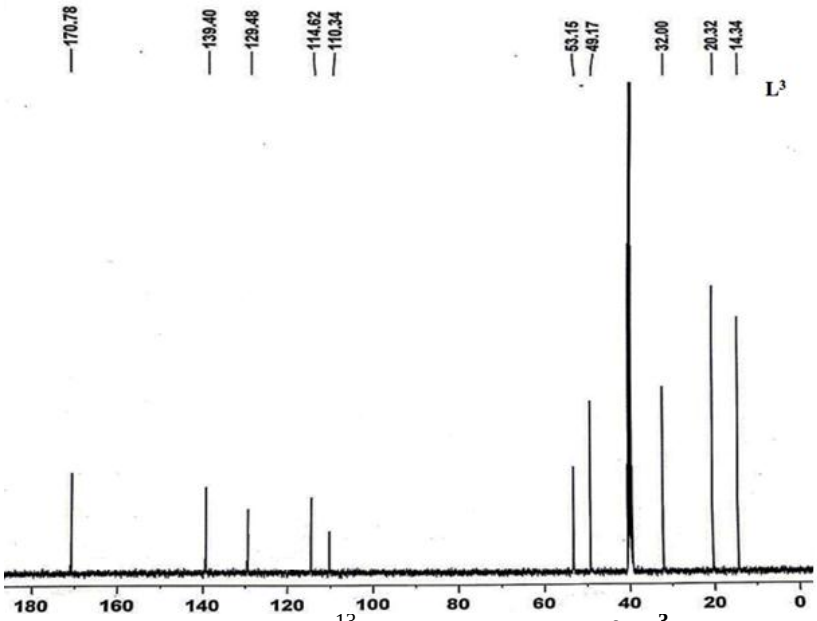

Annexure 26. ^{13}C NMR spectrum of **(L^3)**

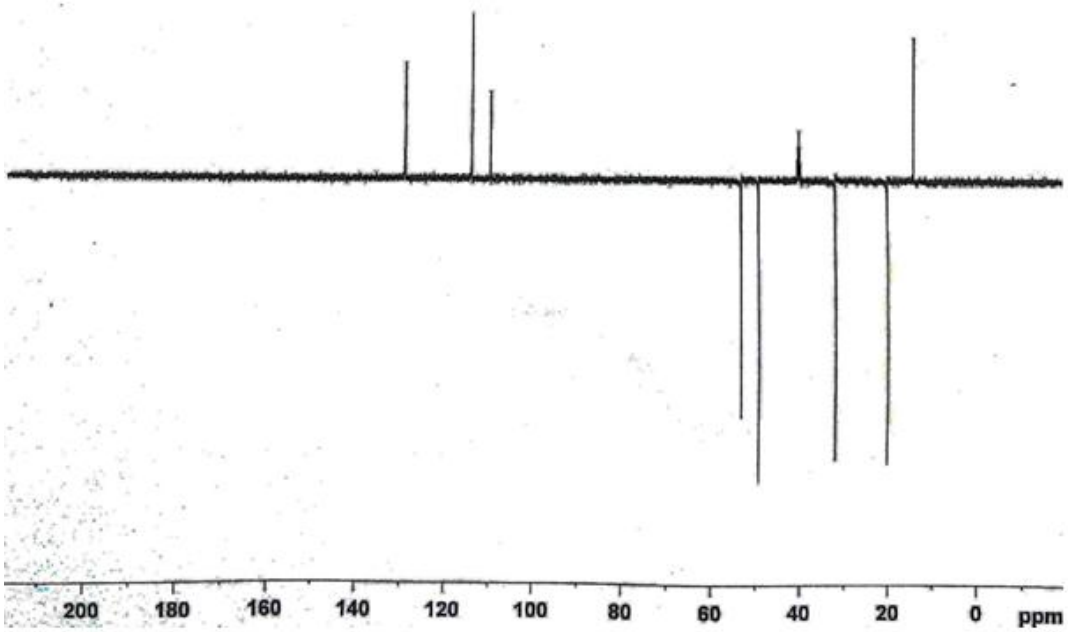

Annexure 27. DEPT 135 NMR spectrum of **(L^3)**

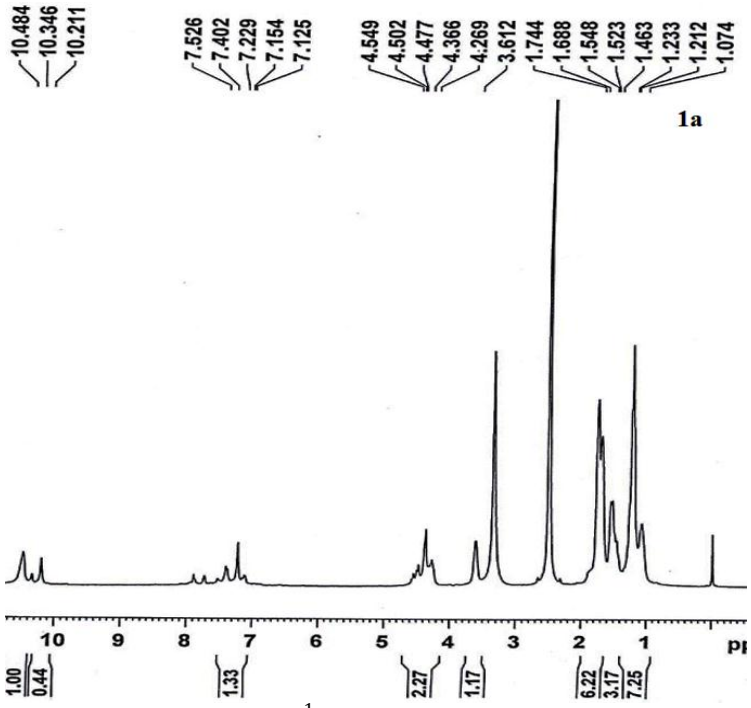

Annexure 28. ^{1}H NMR spectrum of **(1a)**

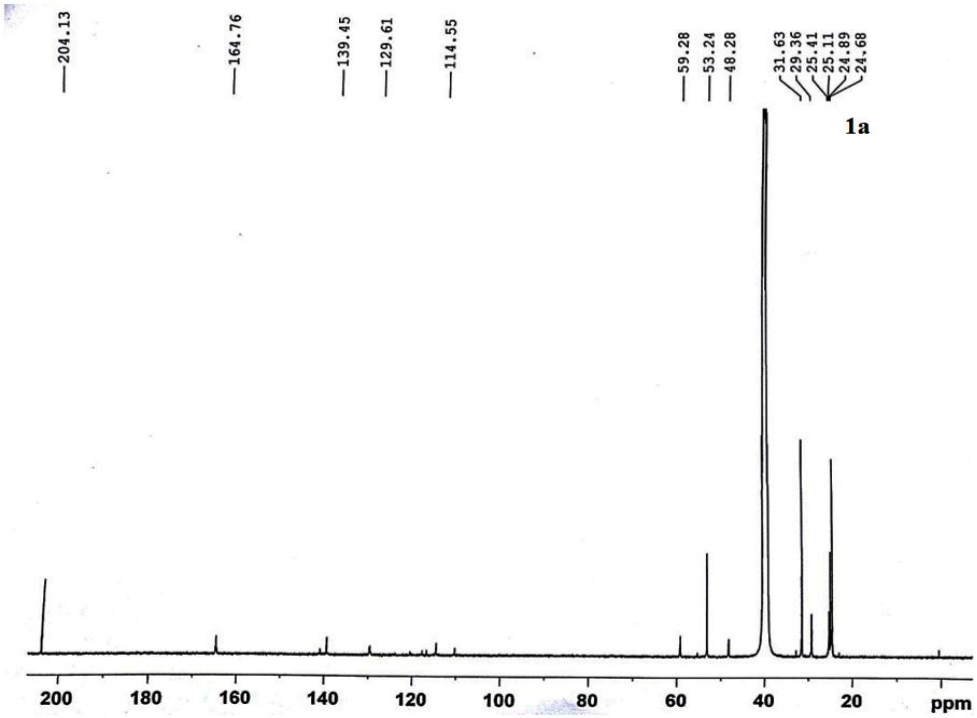

Annexure 29. ^{13}C NMR spectrum of **(1a)**

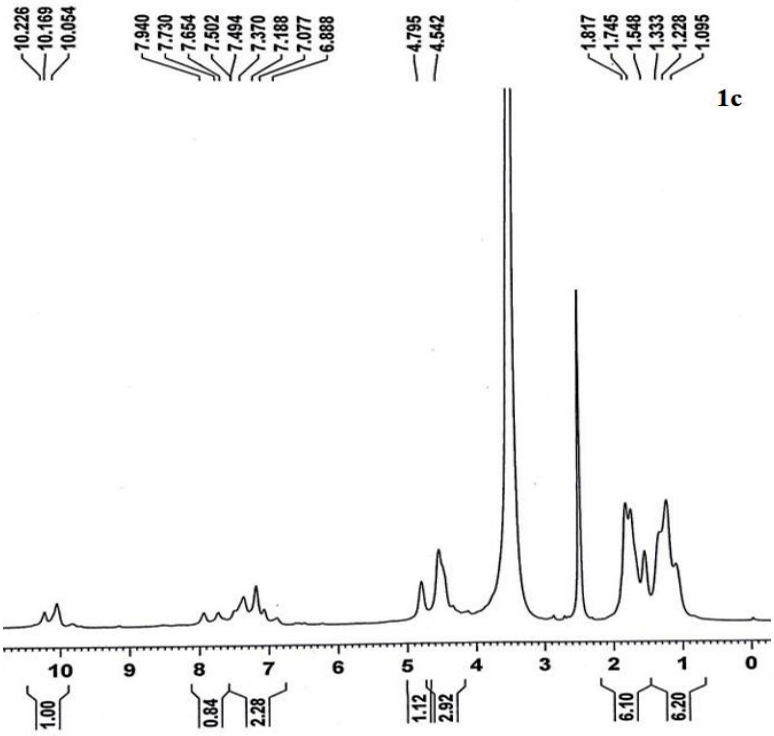

Annexure 30. ^{1}H NMR spectrum of **(1c)**

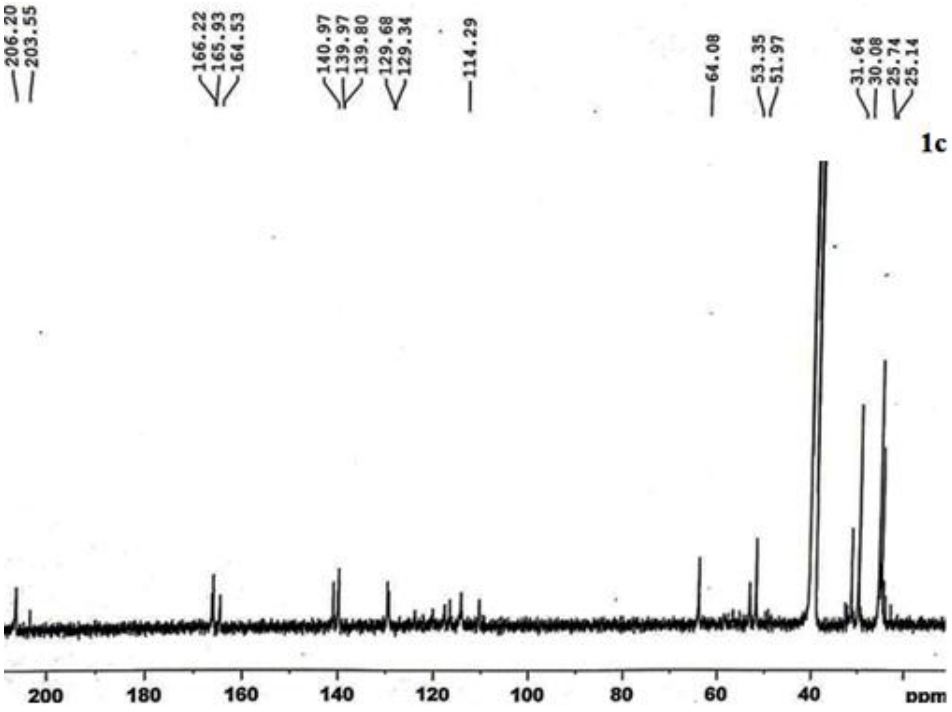

Annexure 31. ^{13}C NMR spectrum of **(1c)**

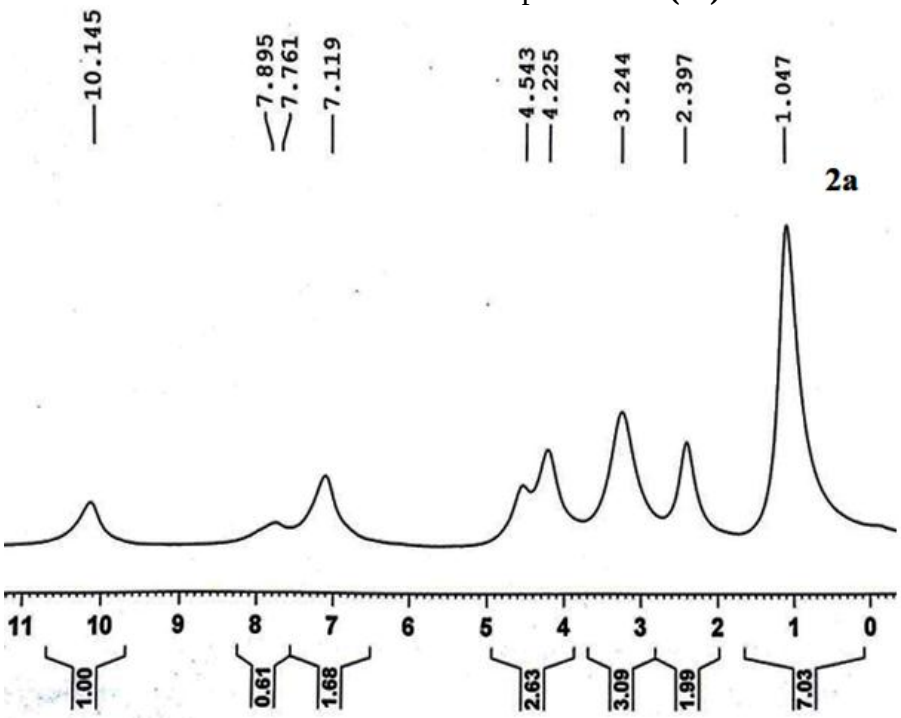

Annexure 32. ^{1}H NMR spectrum of **(2a)**

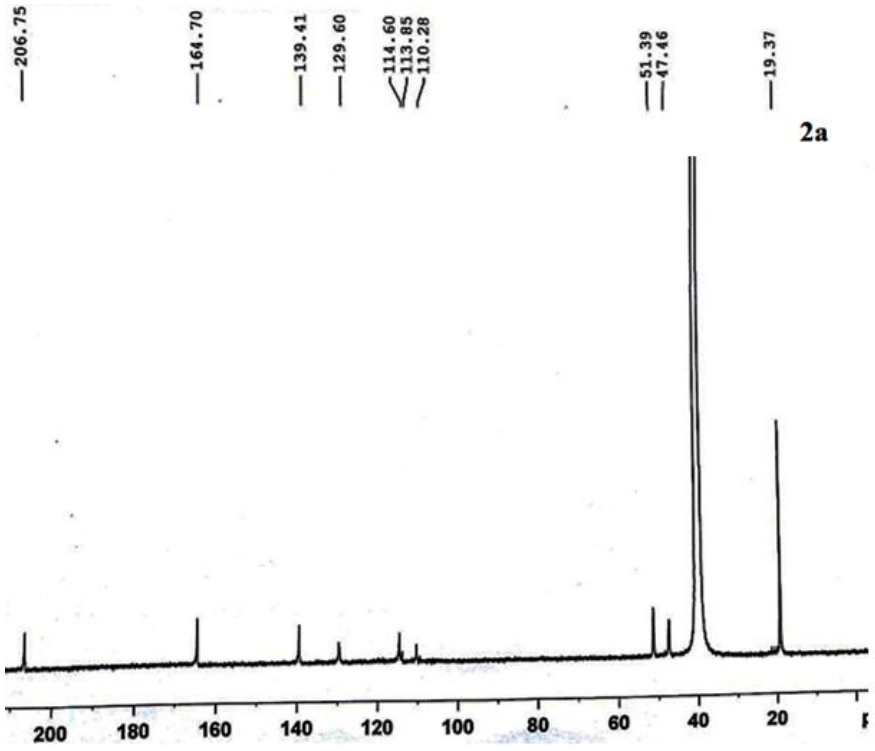

Annexure 33. ^{13}C NMR spectrum of **(2a)**

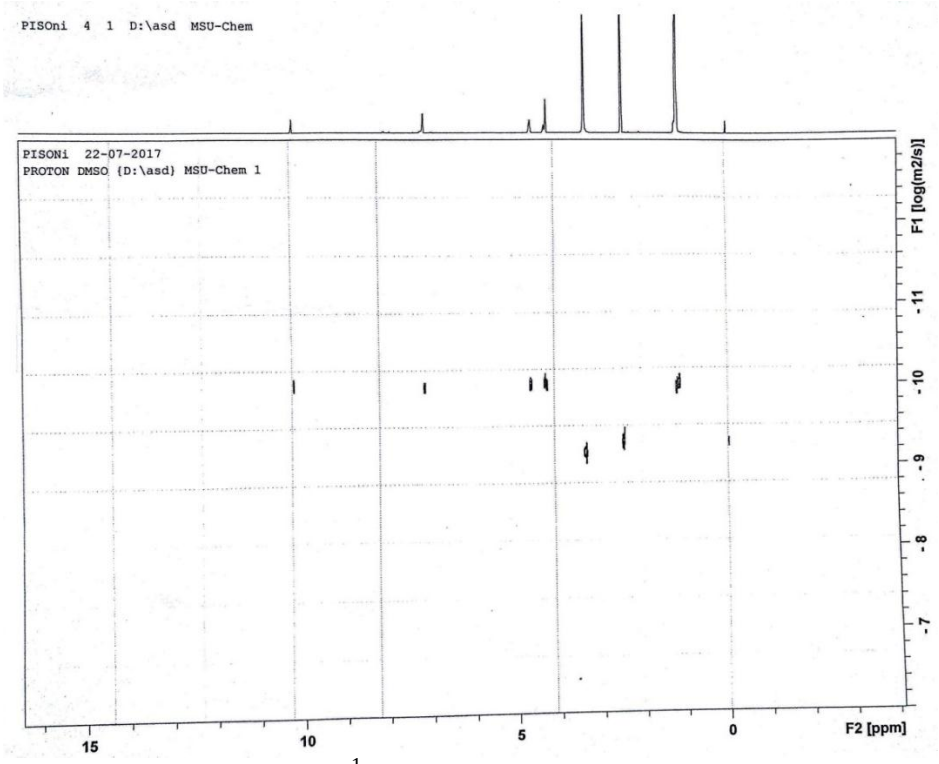

Annexure 34. ^{1}H DOSY NMR spectrum of **(2a)**

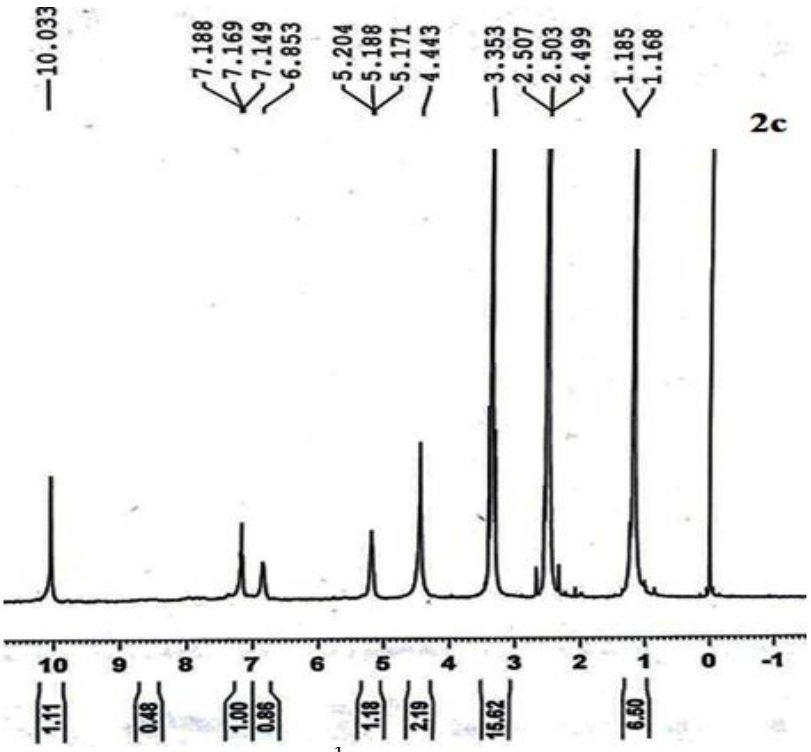

Annexure 35. ^{1}H NMR spectrum of **(2c)**

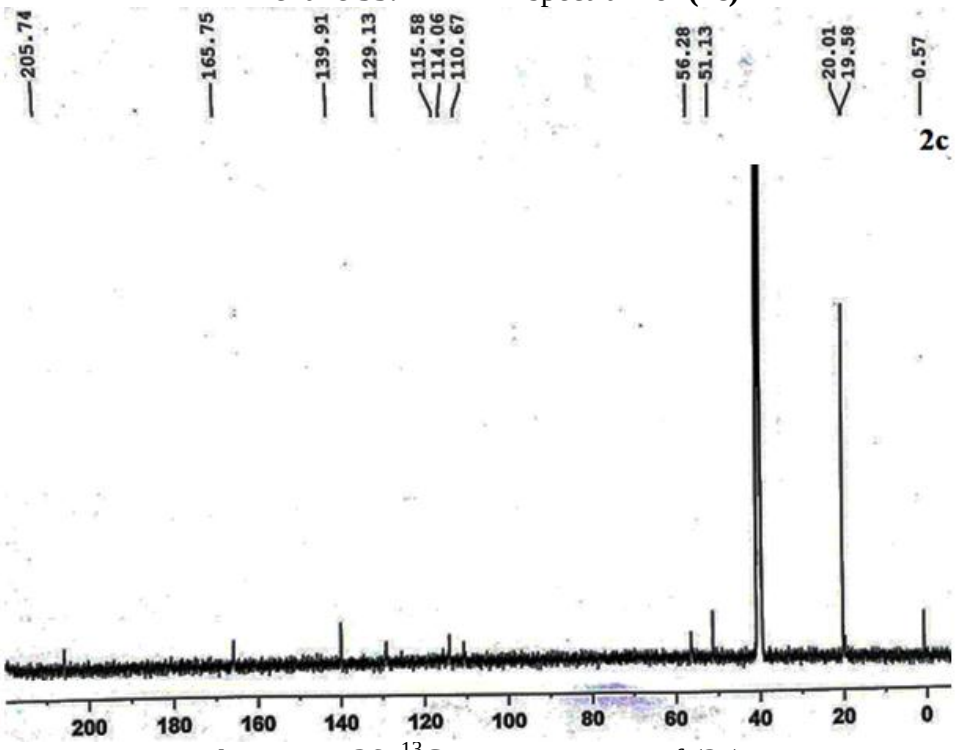

Annexure 36. ^{13}C NMR spectrum of **(2c)**

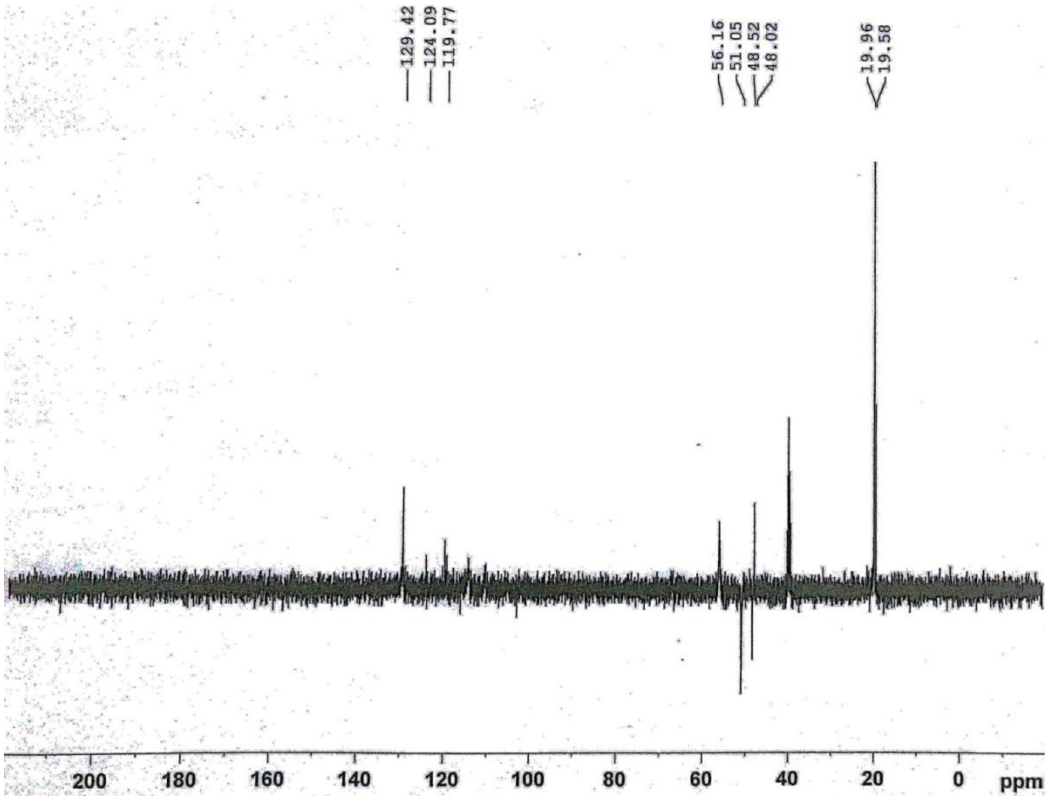

Annexure 37. DEPT 135 NMR spectrum of **(2c)**

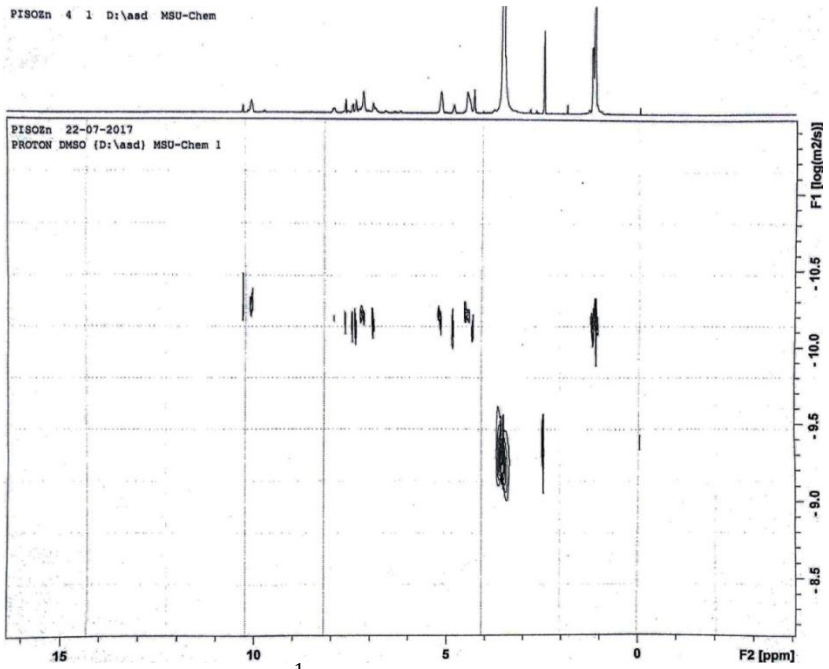

Annexure 38. ^{1}H DOSY NMR spectrum of **(2c)**

UV-visible absorption spectra:

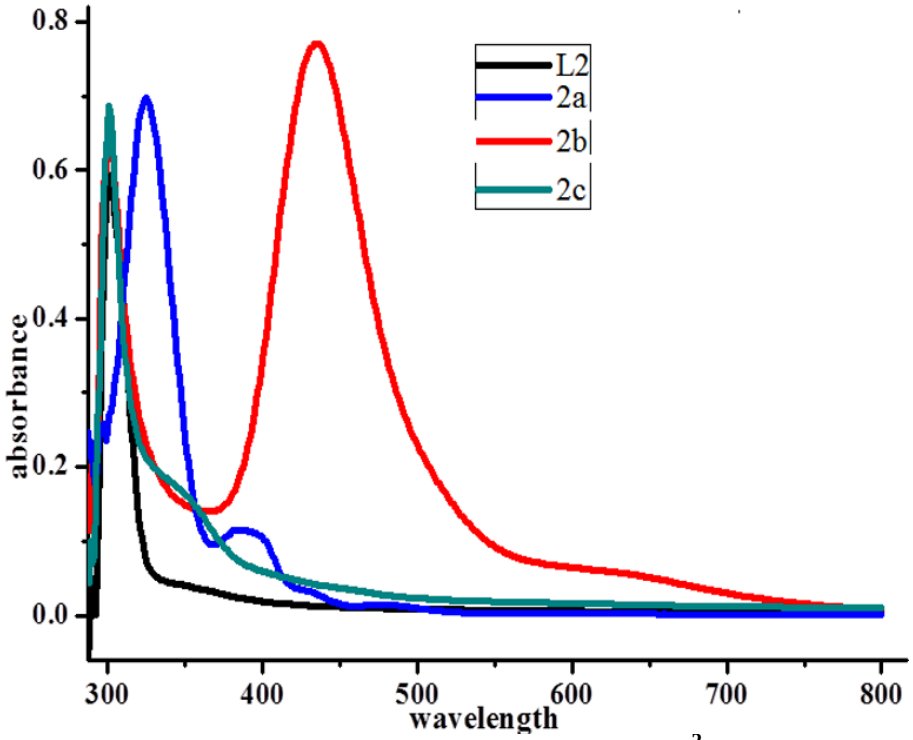

Annexure 39. UV–visible absorption spectra of compounds $\mathbf{L^2}$ and **2a, 2b, 2c** in DMSO solution.

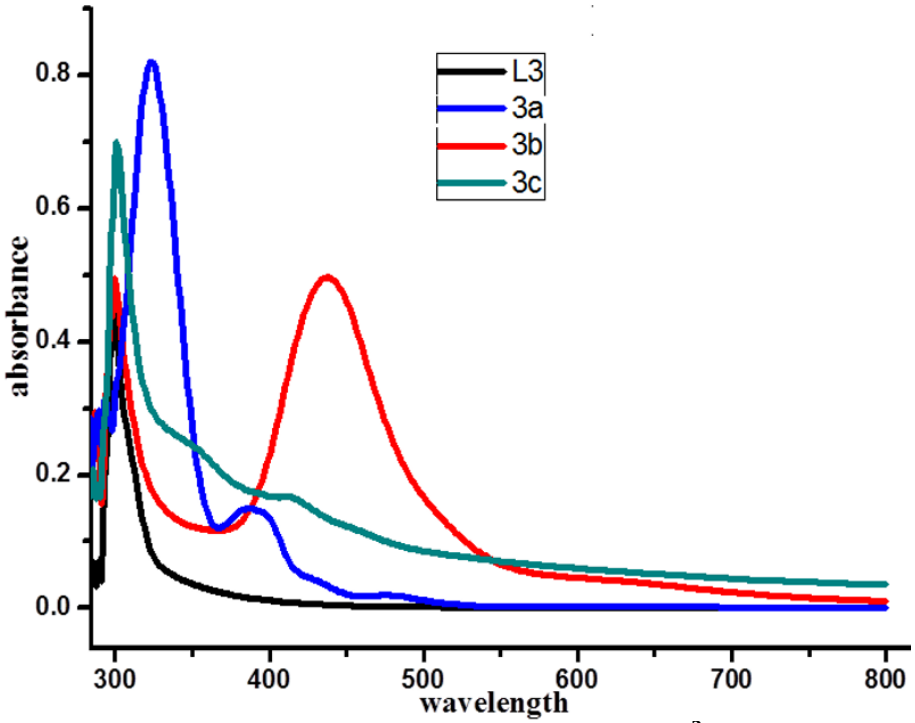

Annexure 40. UV–visible absorption spectra of compounds $\mathbf{L^3}$ and **3a, 3b, 3c** in DMSO solution.

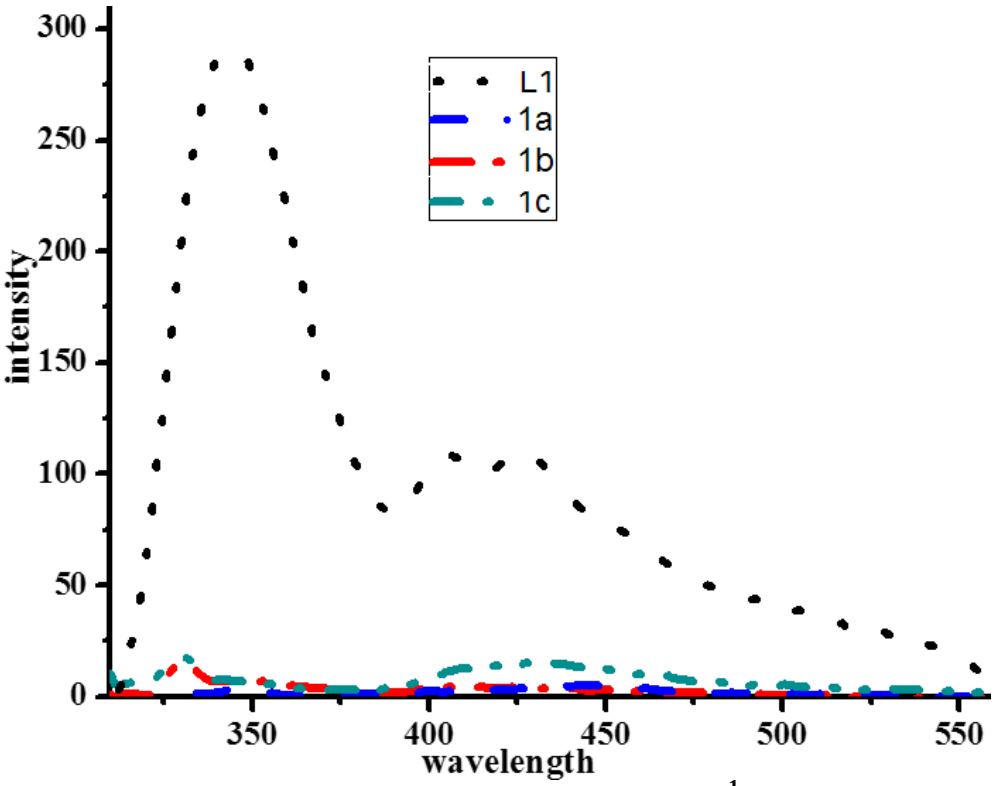

Annexure 41. Fluoresecence emmission spectracompounds **L**[1]and **1a, 1b, 1c** in DMSO solution.

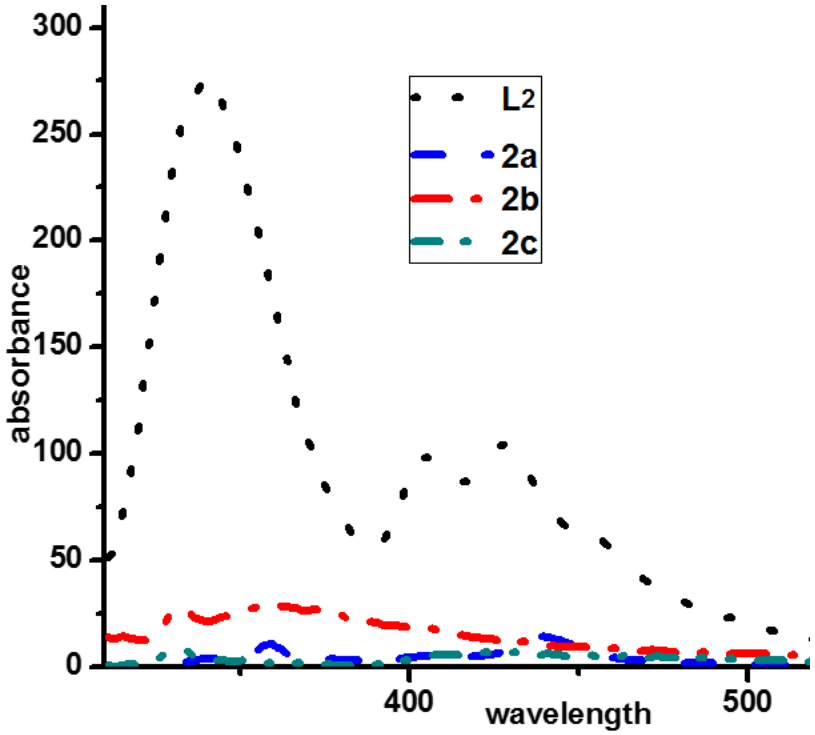

Annexure 42. Fluoresecence emmission spectracompounds **L**[2]and **2a, 2b, 2c**in DMSO solution.

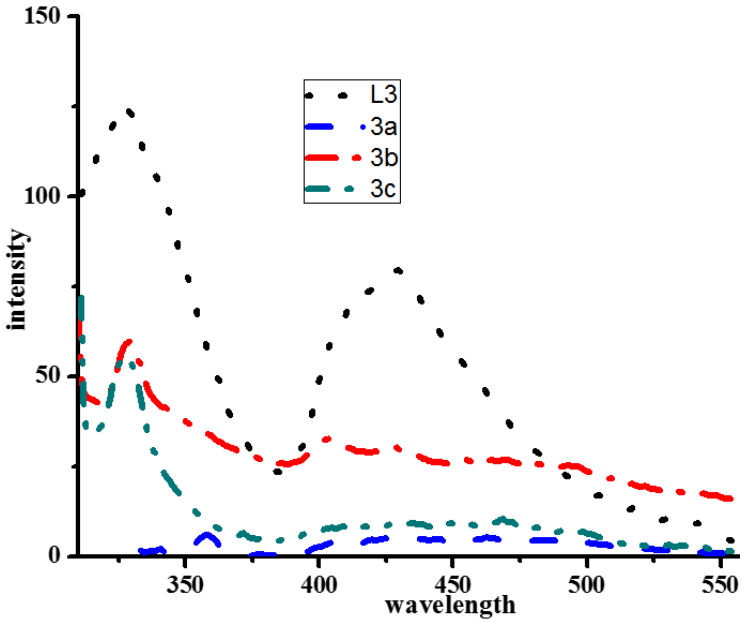

Annexure 43. Fluoresecence emmission spectracompounds $\mathbf{L^3}$and **3a, 3b, 3c**in DMSO solution.

This part of work is under communication: Manuscript ID: QI-RES-10-2017-000655

The additional supporting Information related to this chapter is provided in the CD as follows:

Chapter 4

1. NMR Spectra: **Figure 1-5.**
2. IR Spectra: **Figure 6-9**
3. Thermogravimetric analysis: **Figure 10 and Table 1**
4. Geometry Optimization: **Figure 11-12 and Table 2-6**
5. In vitro cytotoxic study: **Table 7-8** and **figure 13-15**